

Geochemical signatures of redepositional environments: The Namibian continental margin



Michelle L. Abshire^{a,*}, Jeremy D. Owens^b, Jessica Cofrancesco^a, Maik Inthorn^c,
Natascha Riedinger^a

^a Boone Pickens School of Geology, 105 Noble Research Center, Oklahoma State University, Stillwater, OK, 74078, USA

^b Department of Earth, Ocean and Atmospheric Science & National High Magnetic Field Laboratory, Florida State University, Tallahassee, FL 32306, USA

^c Equinor ASA, Martin Linges vei 33, 1364 Fornebu, Oslo, Norway

ARTICLE INFO

Keywords:

Redox
Productivity
Geochemistry
Upwelling
Trace metals
Organic-rich

ABSTRACT

Trace metal abundances in marine sediments have been used extensively to interpret periods of elevated primary productivity and ancient ocean redox conditions. However, sediment reworking that results in post-depositional oxidation, such as bio-irrigation or lateral sediment transport through oxic water, can modify the primary geochemical signal of the sediment, which in turn may impact paleo-redox and/or -productivity interpretations. In the case of sediments on the Namibian Continental Margin (NCM), lateral transport and redeposition contribute to the accumulation of organic matter on the margin slope. To better constrain the geochemical effects of lateral transport on the NCM, we examined the trace metal signature (including solid-phase Fe, Mo, V, Ni, Cu and Ag, and pore-water Fe, Mo, and V) in surface sediments (up to 25 cmbsf) along a transect from shelf to slope through the primary (shelf) and secondary (upper slope) depositional zones of the margin. Despite varying bottom water redox conditions ranging from seasonally anoxic (upper shelf), suboxic (shelf break), and oxic (upper slope), each site has elevated total organic carbon contents (average TOC content of 9.1, 3.2 and 6.8 wt%, respectively), due to high surface water primary productivity and lateral transport of organic-rich material from the shelf to the upper slope. Our results show that the solid-phase contents of the productivity proxies Ni, Cu, and Ag parallel the organic carbon accumulations largely irrespective of the local redox conditions. In contrast, the solid-phase contents of V, Mo, and Fe respond to the local bottom water redox conditions at each site, being enriched under strongly reducing conditions and less-enriched under oxic bottom waters despite enhanced TOC at all three investigated sites. Thus, the enrichment of trace metal and TOC at each site on the NCM can not only be used to reconstruct primary depositional bottom water redox conditions but also to identify zones of sediment redeposition. Using an offshore transect allows for the identification of intense lateral transport and redeposition of organic-rich sediments that are occurring along the margin. The relative concentrations of both redox-sensitive and productivity-related trace metals suggest that the decoupling of trace metals and organic carbon enrichments occasionally observed in the geological record could be explained by the process of lateral transport and redeposition.

1. Introduction

Trace metals have been well-established as redox and/or productivity proxies in sediments and sedimentary rock (Calvert and Pedersen, 1993; Morford and Emerson, 1999; Lipinski et al., 2003; Algeo and Maynard, 2004; Cruse and Lyons, 2004; Borchers et al., 2005; Brumsack, 2006; Piper and Calvert, 2009; Algeo and Rowe, 2012; Owens et al., 2016, 2017) due to the processes responsible for the incorporation of trace metals into sediments and, ultimately, the sedimentary record. Trace metals have three major pathways into the

sediment: 1) the precipitation of seawater sourced metals related to redox conditions (Calvert and Pedersen, 1993; Crusius et al., 1996; Nameroff, 1996; Morford and Emerson, 1999), 2) biologically sourced metals delivered to sediment within organic matter (Algeo and Maynard, 2004; Brumsack, 2006; Piper and Calvert, 2009; Böning et al., 2015), and 3) delivery of metals contained within detrital materials from continental weathering (Emerson and Husted, 1991; Borchers et al., 2005; Tribouillard et al., 2006; Scott et al., 2017) with an important caveat that biologically- and seawater-sourced metals may be difficult to decouple. Trace metals may also be enriched in the sediment

* Corresponding author.

E-mail address: michelle.abshire@okstate.edu (M.L. Abshire).

<https://doi.org/10.1016/j.margo.2020.106316>

Received 29 April 2020; Received in revised form 7 August 2020; Accepted 8 August 2020

Available online 11 August 2020

0025-3227/ © 2020 Elsevier B.V. All rights reserved.

through the exhalation, transport, and oxidation of hydrothermally derived dissolved metals from mid-ocean ridges (e.g., Resing et al., 2015). The variations in total organic carbon (TOC) content and trace metal abundances in the sedimentary record reflect water column productivity and/or the redox state of the bottom water conditions during deposition (Böning et al., 2004, 2005; Borchers et al., 2005; Algeo and Lyons, 2006; Tribouillard et al., 2006; Böning et al., 2015; Little et al., 2015). Thus, variations in trace metal accumulations have been considered relatively reliable proxies that are useful in determining depositional redox and surface water productivity conditions using the concentrations of these elements above detrital background concentrations. Geochemical proxies, however, have some environmental limits on accumulation and may be subject to post-depositional and early/late diagenetic alteration. For example, limited aqueous trace metal supply, which can be due to restricted basin circulation (Algeo and Maynard, 2004; Algeo and Lyons, 2006; Formolo et al., 2014; Zhu et al., 2018), or drawdown of the watermass trace metal inventory due to global redox conditions (Gill et al., 2011; Reinhard et al., 2013; Owens et al., 2016; Sahoo et al., 2016), can mask the geochemical redox signal. Likewise, bioturbation (Aller, 1994; Zheng et al., 2000; Volkenborn et al., 2007) and sediment resuspension (Kowalski et al., 2013) can introduce oxygen into previously anoxic sediments.

1.1. Redox-Sensitive Metals

Redox-sensitive trace metals, such as molybdenum (Mo), iron (Fe), and vanadium (V), are often enriched in organic-rich (> 3 wt% organic carbon) sediment (e.g., Goldschmidt, 1954; Brumsack, 2006 and references therein) and are used in determining modern and ancient depositional redox conditions (e.g. Emerson and Huested, 1991; Calvert and Pedersen, 1993; Algeo and Maynard, 2004; Cruse and Lyons, 2004; Brumsack, 2006; Tribouillard et al., 2006; Lyons et al., 2009; Piper and Calvert, 2009; Algeo and Rowe, 2012; Owens et al., 2016, 2017). Redox conditions such as anoxic, suboxic (dysoxic), and oxic are operationally defined here as having 0.0, 0.0–2.0, > 2.0 mL O₂ L⁻¹ H₂O, respectively (e.g. Tyson and Pearson, 1991). The relative abundance of specific trace metals can assist in differentiating between redox conditions on a local and/or global scale (e.g. Algeo and Maynard, 2004; Tribouillard et al., 2004, 2005; Lyons et al., 2009; Owens et al., 2016; Sahoo et al., 2016). The use of Mo as a redox proxy is based on its distinctive geochemical behavior in both oxic and sulfidic environments (Emerson and Huested, 1991; Algeo and Lyons, 2006). In average shale, approximating typical weathered upper continental crust, Mo is found in very low concentrations (2.6 ppm, Turekian and Wedepohl, 1961; Table A1). On the other hand, Mo is the most abundant transition metal in oxic seawater (Collier, 1985) with the dominant species Mo(VI) in the form of molybdate (MoO₄²⁻). In modern oceans, removal of Mo from oxic seawater occurs via adsorption to Fe- and Mn- (oxyhydr)oxides (Shaw et al., 1990) and the adsorbing particles sink to the seafloor. Under reducing conditions, Fe- and Mn-(oxyhydr)oxide minerals are reduced which releases the adsorbed Mo to the surrounding solution (Shaw et al., 1990; Crusius et al., 1996; Morford and Emerson, 1999). Under sulfidic conditions (available dissolved sulfide), molybdate is fixed as particle-reactive thiomolybdate (MoS_{4-x}O_x²⁻) (Crusius et al., 1996; Helz et al., 1996; Erickson and Helz, 2000; Helz et al., 2011). Sulfidic conditions are favorable for enrichments of Mo to be recorded into the sediment as Mo(IV) (Helz et al., 1996; Erickson and Helz, 2000; Zheng et al., 2000; Poulson Brucker et al., 2009; Helz et al., 2011; Scott and Lyons, 2012). Consequently, Mo accumulations in sediment (> 25 ppm, Scott and Lyons, 2012) have been used in many studies to identify local euxinic (dissolved O₂ = 0 mL L⁻¹ H₂O, plus dissolved sulfide in the water column) environmental conditions with an abundance of dissolved Mo (Helz et al., 1996; Nameroff et al., 2002; Lipinski et al., 2003; Cruse and Lyons, 2004; Borchers et al., 2005; Algeo and Lyons, 2006; Scott and Lyons, 2012).

Vanadium is typically enriched in suboxic and anoxic sediments

(Shaw et al., 1990; Emerson and Huested, 1991). In oxygenated seawater, V exists as V(V), in the form of the vanadate oxyanion and can easily adsorb onto Fe- and Mn-(oxyhydr)oxides (Calvert and Piper, 1984; Wehrli and Stumm, 1989; Emerson and Huested, 1991). Under weakly reducing conditions, V(V) is reduced to particle-reactive V(IV) (McBride, 1979; Wanty and Goldhaber, 1992) and forms vanadyl ions, hydroxyl species, and insoluble hydroxides (Van der Sloot et al., 1985). In the presence of dissolved sulfide under strongly reducing conditions, V(IV) is further reduced to V(III) and precipitated as insoluble oxyhydroxides (Breit and Wanty, 1991; Emerson and Huested, 1991; Wanty and Goldhaber, 1992). Because of the two-step reduction process necessary for V fixation in the sediment, V concentrations, when combined with Mo concentrations, are used to identify anoxic and euxinic environments at local and, potentially, global scales (Algeo and Maynard, 2004; Owens et al., 2016).

In oxic seawater, Fe and Mn precipitate as Fe and Mn oxyhydroxides, thus dissolved Fe and Mn are often found in concentrations below 1 nM (Bruland and Lohan, 2006, and references therein). However, hydrothermally-derived dissolved Fe and Mn concentrations can be higher near hydrothermal systems (Saito et al., 2013; Resing et al., 2015). Due to the behavior of Fe under various redox conditions, the presence of dissolved Fe in pore-waters, solid-phase total Fe content, and the Fe/Al ratio, which records reactive Fe enrichment (Werne et al., 2002; Lyons et al., 2003; Little et al., 2015; Raiswell et al., 2018), are commonly used as redox indicators in marine environments (Raiswell and Berner, 1985; Lyons et al., 2003; Cruse and Lyons, 2004; Lyons and Severmann, 2006; Raiswell et al., 2018). Sediments with Fe/Al ratios above the threshold value of 0.66 are considered to be enriched over oxic marine sediments, which contain Fe/Al ratios of approximately 0.55 (Raiswell et al., 2018), reflecting deposition in an anoxic and/or sulfidic environment, such as the Black Sea (Lyons and Severmann, 2006).

Some Fe may be mobilized from suboxic to anoxic sediments, transported, and sequestered during Fe sulfide precipitation in a euxinic water column as pyrite. Based on this process, transport of reactive Fe from the shelf downslope has been observed in the Black Sea (Severmann et al., 2008) and the Peruvian continental margin (Scholz, 2018). Surface sediments within an OMZ are subject to diffusive loss of Fe (Scholz et al., 2011), and Peruvian margin sediments within the OMZ show Fe depletion. Some of the dissolved Fe (and Mn) are then re-precipitated at the boundaries of the OMZ (Scholz et al., 2011; Scholz et al., 2014).

1.2. Productivity-related trace metals

Productivity-related trace metals accumulate in sediments deposited under upwelling waters due to a high flux of organic matter with enhanced organic carbon preservation at depth (e.g. Böning et al., 2004). Metals such as nickel (Ni), copper (Cu), and silver (Ag) are generally associated with biocycling processes and bioproductivity (Bruland, 1983; Borchers et al., 2005) and are primarily delivered to marine sediments directly within, or adsorbed to (post-mortem), sinking biodebris (e.g. Brongersma-Sanders et al., 1980; Böning et al., 2015).

Under oxic conditions, Ni is primarily preserved as soluble Ni-carbonate (NiCO₃) or adsorbed to humic and fulvic acids, however, Ni may also be present as soluble Ni²⁺ cations or NiCl⁺ ions (Calvert and Pedersen, 1993; Whitfield, 2002; Algeo and Maynard, 2004). Copper is typically present in oxic settings as organometallic ligands and, to a lesser degree, as soluble CuCl⁺ ions (Calvert and Pedersen, 1993; Whitfield, 2002; Algeo and Maynard, 2004). The productivity-related trace metals incorporated into sediments of upwelling margin settings, such as the Chilean and Peruvian margins, are primarily pre-concentrated in, or adsorbed onto, biodebris and delivered to the sediments by settling through an oxygen minimum zone (OMZ; Böning et al., 2004, 2005). As organic matter degrades, incorporated metals, such as Ni and Cu, are released into pore-waters (Moore et al., 1988).

Under sulfidic conditions, pore-water Ni and Cu may be incorporated into sediment as insoluble sulfides (Moore et al., 1988; Huerta-Diaz and Morse, 1990, 1992; Morse and Luther, 1999), and remain in the sediment.

While present understanding of the marine geochemical cycling of Ag is relatively limited, when compared to some other trace metals, several studies have demonstrated that elevated Ag content in sediment can be used as a reliable indicator of ocean surface productivity (Crusius and Thomson, 2003; Friedl and Pedersen, 1998, 2001; Hendy and Pedersen, 2005; McKay and Pedersen, 2008; Wagner et al., 2013; Chang et al., 2015). Similar to Ni and Cu, Ag is taken up in the bodies of micro-organisms in surface waters (Fisher and Wente, 1993) or adsorbed to organic matter from seawater and delivered to the seafloor along with the sinking biodebris (Friedl and Pedersen, 1998; Böning et al., 2004). In the East Atlantic Ocean waters, dissolved Ag correlates with silica (Flegel et al., 1995) and increases with water depth (Martin et al., 1983). A study by Morford et al. (2008) demonstrated a similar increase in dissolved Ag with water depth, despite carbon flux being greatest at locations under a shallow water column. This increase of Ag in sediments under deeper water columns has been observed in sediments from the Western Canadian, Mexican, Peruvian (McKay and Pedersen, 2008), and Chilean (Böning et al., 2005; McKay and Pedersen, 2008) continental margins. These observations are similar to barium (Ba) as a productivity indicator, where Ba is scavenged within the water column requiring certain water column depths to appropriately represent organic carbon accumulation in the sediments (e.g. Dymond et al., 1992; Von Breyann et al., 1992; Klump et al., 2000; Nameroff et al., 2002; McKay and Pedersen, 2008; Horner et al., 2015). Due to the nutrient-type distribution of Ba and Ag in the water column (Bruland and Lohan, 2006, and references therein), concentrations are greater in deeper waters. Thus, the amount of Ag scavenged by sinking particulate organic matter is related to the availability of Ag with increasing water depth, as well as particle travel time through the water column. Additionally, in highly-reducing conditions, Ag can form Ag_2S , which is an extremely insoluble sulfide (Dyrssen and Kremling, 1990; Friedl and Pedersen, 2001) and is found enriched in sulfidic sediment through this reduction pathway. To determine the effects of redeposition on a suite of redox-sensitive and productivity-related trace metal signals, we present with this study the solid-phase and pore-water trace metal (TM_{PW}) geochemistry of sediments on the NCM. A combined approach of redox-sensitive and productivity-related trace metal analysis and total organic carbon content measurements can provide useful insights to aid in paleoenvironmental reconstructions of organic-rich depositional systems to identify ancient environments that may have experienced sediment redeposition.

2. Methods

2.1. Study area

Along the Namibian Continental Margin (NCM), southeasterly trade winds induce upwelling of nutrient-rich deep waters (e.g. Shannon and Nelson, 1996), which are delivered to the photic zone. The perennial upwelling along the NCM induces strong primary production (Mollenhauer et al., 2002), which is estimated at a rate of 0.37 Gt carbon per year (Carr, 2001). The highest productivity is located in waters above the shelf with additional high productivity in filaments of nutrient-rich water that extends seaward above the continental slope (Carr, 2001, Mollenhauer et al., 2002). The degradation of a large quantity of sinking biodebris creates extreme water column oxygen depletion and periodic sulfidic bottom water (Borchers et al., 2005). The resulting OMZ stretches from the shelf, across the upper continental margin and beyond the shelf break (Chapman and Shannon, 1985). Within the OMZ, oxygen-deficient conditions augment the preservation of large quantities of organic carbon in the sediment (van der Weijden et al., 1999). The core of the OMZ offshore Namibia is at ~200 m water

depth (e.g. Brüchert et al., 2003; Inthorn et al., 2006a), however, seasonal variability in the upwelling cells responsible for the high primary productivity in NCM waters results in the OMZ layer becoming less-pronounced during the austral winter/spring (Monteiro et al., 2006; Böning et al., 2020). Likewise, the OMZ expands during the highly-productive summer months (Brüchert et al., 2003; Monteiro et al., 2006; Böning et al., 2020). The strong coastal upwelling and high primary productivity have been occurring in this region since at least the early Pleistocene (Berger and Wefer, 2002).

The phytoplankton that thrives in the coastal waters above the Namibian shelf is dominated by diatoms, dinoflagellates, and radiolarians (Summerhayes et al., 1995) resulting in shelf sediments consisting primarily of organic carbon-rich diatomaceous ooze (Bremner, 1983; Summerhayes et al., 1995; Mollenhauer et al., 2002). Waters above the shelf break and upper slope contain an abundance of coccolithophores and foraminifera (Giraudeau et al., 1993) delivering a small, but not negligible, amount of carbonate and organic material to the sediments below (McPhee-Shaw et al., 2004; Inthorn et al., 2006b). Previous studies have used optical measurements (Inthorn et al., 2006a) and ^{14}C dating of suspended organic carbon (Inthorn et al., 2006b) to monitor the movement and transport of sediments along the NCM. The Inthorn et al. (2006a, 2006b) studies revealed that the downslope trends in organic carbon accumulation, lability, and ^{14}C ages are explained by the extensive particle transport occurring along the NCM in nepheloid layers, which are discrete layers of water with enhanced particle content relative to surrounding waters. In the NCM, organic-rich particles from sediments below the highly productive shelf waters are transported offshore in nepheloid layers. This lateral transport and redistribution of particles create a secondary area of intense organic carbon accumulation on the upper slope (Inthorn et al., 2006a, 2006b; Mollenhauer et al., 2007). The shelf and upper slope are separated by the shelf break where radiocarbon dating (Mollenhauer et al., 2002; Inthorn et al., 2006b) and parasound sediment echosounder profiles (Mollenhauer et al., 2007) revealed an erosive regime, which exposes significantly older sediments compared to the shelf. Erosion along the shelf break is also mirrored in the increased intensity of the bottom nepheloid layer near the shelf break, with estimated suspended particulate concentrations up to 2.1 mg L^{-1} based on beam attenuation and light scattering (Inthorn et al., 2006a). The intermediate nepheloid layer which extends across the upper slope, where it diminishes in intensity, is indicative of sediment resuspension and transport to the upper slope depocenter (Inthorn et al., 2006a; Mollenhauer et al., 2007). Furthermore, Inthorn et al. (2006b) found that the ^{14}C ages of suspended material collected from bottom nepheloid layers (within 0.3 m of the seafloor) along three offshore transects is very similar in age to nearby core-top sediments which are progressively older offshore; around 0.125 kyr. on the shelf (Mollenhauer et al., 2002), 2.94 kyr. on the shelf break, and 3.11 kyr. on the upper slope (Mollenhauer et al., 2007). The overall modern sedimentation rates on the NCM are high with estimates from $\geq 100 \text{ cm kyr}^{-1}$ on the shelf, mainly due to the high primary productivity in surface waters (Bremner and Willis, 1993; Mollenhauer et al., 2002), to $5\text{--}17 \text{ cm kyr}^{-1}$ on the upper slope (Mollenhauer et al., 2002), where sediments are primarily composed of resuspended material (Mollenhauer et al., 2007).

A previous study by Abshire et al. (2020) examined the shelf, shelf break, and upper slope sediments of the NCM and found a pronounced decoupling of the redox-sensitive trace metal uranium (U) and TOC in redeposited sediments on the upper slope. It was concluded that the loss of U from the organic-rich sediments occurred during offshore transport and redeposition. Uranium isotope evidence confirmed that the sediments were initially deposited under anoxic conditions and were subjected to post-depositional oxidation, which led to a loss of U from the organic-rich sediments. The erosion, lateral transport, and redeposition of sediments on the NCM make this the ideal area to investigate the impact of dynamic depositional conditions in organic-rich sediments on the trace metal inventory.

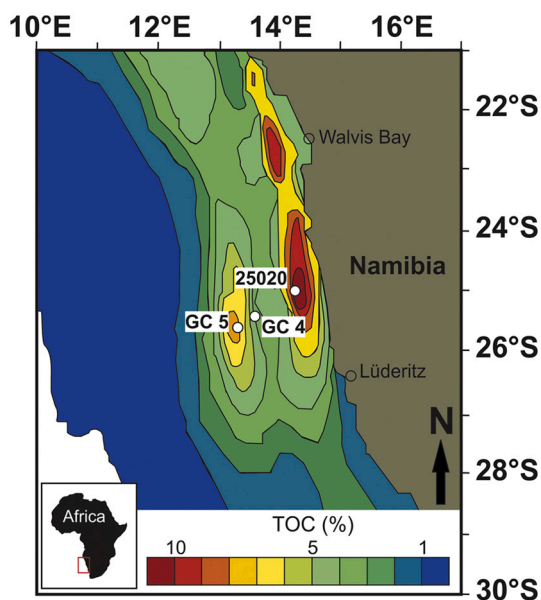


Fig. 1. Map of the study area showing the areas of intense organic carbon preservation (warmer colors) in the sediments (modified after Mollenhauer et al., 2002). Sample sites 25020 (shelf), GC 4 (shelf break), and GC 5 (upper slope) are labeled as white circles.

2.2. Sampling

Sediment cores were collected for geochemical analyses from the NCM offshore southwestern Africa (Fig. 1) onboard the research vessel RV MIRABILIS as part of the May 2015 Regional Graduate Network in Oceanography (RGNO) program. Cores 25020, GeoChemistry_4 (GC 4), and GeoChemistry_5 (GC 5) were collected from the outer shelf, shelf break, and upper slope, respectively. Surface sediment cores were retrieved from the three sample sites using a multi-corer (MUC) device (Table 1). Bottom water was immediately extracted from the top of the core using a syringe and cores were immediately sliced onboard the ship into 1–2 cm intervals. Sediments were transferred into centrifuge tubes, and the headspace was purged with nitrogen gas. Pore-waters were then extracted from each tube containing sediments via clean Rhizons (Seeberg-Elverfeldt et al., 2005), which were soaked in milliQ water prior insertion, connected to a 30 mL syringe through an airtight and pre-drilled hole in the top of each centrifuge tube. The first mL of extracted liquid was discarded to prevent oxidation and dilution. All extracted water samples were acidified with concentrated trace metal grade (TMG) nitric acid at a concentration of 20 $\mu\text{L}/\text{mL}$ of sample and were stored at 4 °C.

2.3. Aqueous phase Analysis

Measurements of ocean water temperature, salinity, and bottom water oxygen levels were obtained from the research vessel using a Conductivity Temperature Depth (CTD) device with an oxygen sensor that had a detection limit of 0.05 $\text{mL O}_2 \text{ L}^{-1} \text{ H}_2\text{O}$.

Table 1

Location, water depth, bottom water oxygen concentration, and depositional redox environment for sites 25020 (shelf), GC 4 (shelf break) and GC 5 (slope).

| Core name | Latitude | Longitude | Water depth (m) | Bottom water oxygen (mL L^{-1}) | Depositional Environment |
|-----------|------------|------------|-----------------|--|--------------------------|
| 25020 | 25°00.00'S | 14°28.20'E | 116 | < 0.05 [#] | Anoxic outer shelf |
| GC 4 | 25°20.66'S | 13°46.48'E | 302 | 1.11 | Suboxic shelf break |
| GC 5 | 25°30.00'S | 13°27.00'E | 795 | 3.36 | Oxic upper slope |

Samples were collected in May 2015. Anoxic, suboxic, and oxic conditions in the bottom waters (< 1 m above sea floor) of the NCM have been previously defined in Abshire et al. (2020).

[#] CTD detection limit is 0.05 mL L^{-1} .

Bottom and pore-water samples were analyzed for trace metal concentrations using an inductively-coupled plasma-mass spectrometer (ICP-MS, ThermoFisher Scientific, iCAP Qc) at Oklahoma State University. Sample aliquots were diluted 25-fold with 2% supra-pure nitric acid prior analysis. A standard reference material NIST 1643f was analyzed with each set of samples for quality control. The standard deviation for all elements was better than 5%. All generated pore-water data are summarized in Table A2.

2.4. Solid-phase analysis

Total organic carbon (TOC) content of the NCM sediment was measured using an Elemental Analyzer (EA, Costech) at Oklahoma State University (OSU). Standard reference material USGS-40 was run alongside samples with an error of less than 1%. The TOC data used in this study and details of the methods have been previously published in Abshire et al. (2020).

Samples for analyses of Al, Mn, Fe, V, Mo, Ni and Cu from all cores were completely digested using a CEM Mars 6 microwave with 5 mL of ~9 M trace metal grade (TMG) nitric acid to remove organic matter followed by concentrated TMG hydrochloric, nitric, and hydrofluoric acids (e.g. Them et al., 2017). Sample preparation and analyses on a Thermo Element II ICP-MS were carried out in the Geochemistry group at the National High Magnetic Field Laboratory at Florida State University. A set of standard reference materials (NIST 2702, USGS SDO-1, and USGS SCO-1) were digested and analyzed with each set of samples and, in all cases, reported elemental concentrations were within the published analytical error. Duplicate analyses of NIST 2702 had relative standard deviations < 2%, with the exception of Al (RSD = 8%) and Mo (RSD = 3.5%).

Samples analyzed for Ag content from all cores underwent a modified temperature and pressure digestion protocol using a PicoTrace digestion system (after after Steinmann et al., 2020) with concentrated TMG nitric, hydrofluoric, and perchloric acids in PTFE vials. Samples were heated to 170 °C until fully dissolved and then evaporated until dry. Residues were dissolved in 5% TMG nitric acid. The Ag content was measured on a ThermoScientific iCAP Qc ICP-MS at OSU. Standard reference material NIST SRM 2702 was digested and analyzed alongside samples with less than 3% error and 1.4% RSD between duplicate standards.

Since Al can be used as an indicator of the aluminosilicate fraction of a sedimentary deposit, indicating the extent of input from continental weathering (e.g. Brumsack, 1989; Calvert and Pedersen, 1993; Morford and Emerson, 1999; Piper and Perkins, 2004), Trace metal/Al (TM/Al) ratios will be reported alongside trace metal data. Additionally, enrichment factors (EF) for each solid-phase element were calculated based on the average enrichment at each site, relative to average shale composition as defined by Turekian and Wedepohl (1961 Table A1) (e.g. Borchers et al., 2005; Brumsack, 2006; Bennett and Canfield, 2020). The calculation for EFs is as follows:

$$EF_{\text{TM}} = (\text{TM}/\text{Al})_{\text{sample}}/(\text{TM}/\text{Al})_{\text{shale}} \quad (1)$$

All generated solid-phase data are summarized in Table A3 (TOC and CaCO_3) and Table A4 (solid-phase trace metals).

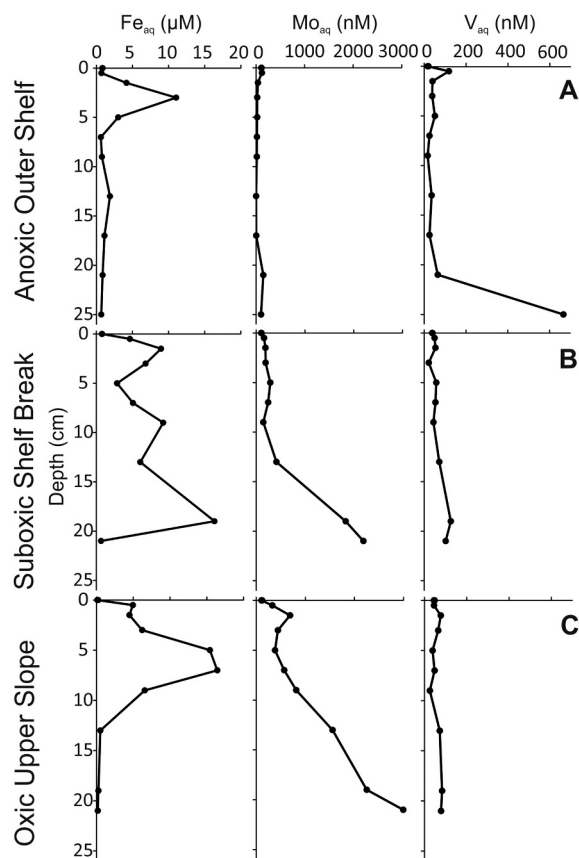


Fig. 2. Aqueous (aq) concentration of iron (Fe), molybdenum (Mo) and vanadium (V) from sediment cores collected from the A. anoxic shelf (site 25020), B. suboxic shelf break (site GC 4), and C. oxic upper slope (site GC 5). Pore-water Ni and Cu were measured and were below detection limit in all sampled pore-waters. Samples at 0 cmbsf are bottom water samples.

3. Results

3.1. Aqueous phase

All pore and bottom water trace metal data from sites 25020 (shelf), GC 4 (shelf break), and GC 5 (slope) are listed in the appendix, Table A2, and are shown in Fig. 2. At all three study sites, bottom and pore water Ni and Cu were below detection limits of 0.08 ppb and 0.22 ppb, respectively. In the bottom water (0 cmbsf) at the shelf site (25020) the concentration of dissolved Fe is $< 1 \mu\text{M}$ and increases to $\sim 11 \mu\text{M}$ by a depth of 3 cmbsf, followed by a decrease downcore to $< 1 \mu\text{M}$ at 25 cmbsf. The concentration of Mo is 107–114 nM in the bottom water, with a slight increase of Mo_{PW} to $\sim 120 \text{ nM}$ at 0.5 cmbsf then decreases into the sediments to 1 nM by 13 cmbsf. At 17 cmbsf the concentration of Mo_{PW} begins to increase to 151 nM by 21 cmbsf. At 25 cmbsf the concentration of Mo_{PW} is 107 nM. The dissolved V concentration in the bottom water is $< 20 \text{ nM}$ increasing to 117 nM into the core top pore waters. At a depth of 3 cmbsf the concentration of V_{PW} drops to 38 nM, followed by fluctuations between 17 and 65 nM downcore. At the core bottom, the V_{PW} concentration spikes to 664 nM (Fig. 2A).

At the shelf break (site GC 4) Fe_{PW} concentration fluctuates between 3 and 9 μM down to 13 cmbsf, followed by an increase downcore to 16 μM at 19 cmbsf. At the core bottom Fe_{PW} decreases to $< 1 \mu\text{M}$. The concentration of Mo in the bottom water of core GC 4 is 106–111.5 nM, and increases in the sediment pore-waters to 292 nM by 5 cm core depth. From 7 to 9 cmbsf the Mo_{PW} concentration decreases to 145 nM, before increasing sharply to 2208 nM by the core bottom. Dissolved V concentrations are $\sim 40 \text{ nM}$ in the bottom water, increase to 54 nM at

1.5 cmbsf, then decrease to 22 nM by a depth of 3 cmbsf, followed by an increase to 58 nM by a depth of 5 cmbsf, and a decrease to 44 nM by 9 cmbsf (Fig. 2B). From 13 to 19 cmbsf the V_{PW} concentration increases to 127 nM before decreasing to 103 nM by the core bottom (Fig. 2B).

The concentration of Fe is $< 1 \mu\text{M}$ in the bottom water of site GC 5 (upper slope), increasing to 5 μM at 3 cm, before spiking to 16 μM at 7 cmbsf. The Fe_{PW} concentration decreases with depth to 0 μM at 19 cmbsf. Dissolved Mo in the bottom water is 103–124 nM and Mo_{PW} increases rapidly to 354 nM in the core top to 693 nM by a depth of 1.5 cmbsf, followed by a drop to 385 nM at 5 cmbsf. The Mo_{PW} concentration increases again reaching 3033 nM at 21 cmbsf. The concentration of V in the bottom water is 44–47 nM and increases in the pore-water to 77 nM at 1.5 cmbsf, followed by a decrease to 38 nM at 5 cmbsf. From 7 to 9 cmbsf the concentration of V_{PW} fluctuates before increasing to 83 nM by 19 cmbsf and decreases again to 78 nM at the core bottom.

3.2. Solid-phase

The sediments from the outer shelf (site 25020) are finely-laminated and green to black in color with a strong sulfur odor. Sediments on the shelf break are brown to black colored with no visible laminations, and upper slope sediments are non-laminated and green to black in color.

3.2.1. Organic and inorganic carbon

All organic carbon (TOC) data included in this manuscript were previously reported by Abshire et al. (2020). Carbonate (CaCO_3) data are new to this study and are presented in the appendix in Table A3. The upper 10 cm of shelf sediments have TOC content of 7.2–8.8 wt% which increases to 11.5 wt% TOC at 25 cmbsf. The CaCO_3 content at this site ranges between 7.1 and 17.1 wt% with shell fragments observed in the bottom half of the core (Fig. 3A). Sediments from the shelf break have an average of 3.2 wt% TOC and CaCO_3 amounts range from 22.7–36.1 wt% (Fig. 3B). Upper slope sediments contain 5.8–7.8 wt% TOC, with CaCO_3 contents ranging from 34.7–63.0 wt% with shell fragments observed throughout the core (Table A3, Fig. 3C).

3.2.2. Al, Mo, V, Mn and Fe

The contents of solid-phase metals from cores 25020, GC 4 and GC 5 (Table A4) are each plotted against Al (Fig. 3) to normalize the data against the lithogenic background (e.g. Calvert and Pedersen, 1993). All sediments from the shelf (site 25020) generally have increasing metal content with depth. The Al contents of the shelf sediment range from 0.7 wt% to 2.3 wt%. Mo content is lowest (14.9 ppm) at the core top and increases to 38.2 ppm at a depth of 25 cmbsf. Solid-phase V content is 38.5 ppm at the core top, decreases slightly to 28.9 ppm (at 3 cmbsf) then increases again to 55.1 ppm (9 cmbsf). Beyond 9 cmbsf, V content decreases again to 48 ppm before increasing significantly to 124.3 ppm at the core bottom. The Mn and Fe content of the shelf sediment generally increase down core from 38 ppm Mn and 0.5 wt% Fe at the core top to 160 ppm Mn and 1.8 wt% Fe at the core bottom.

Sediments at site GC 4 on the shelf break has Al content ranging from 1 wt% to 1.4 wt% and Mo content between 3 and 8 ppm that increases slightly with depth in the sediment. Like Mo, V generally increases with depth from 31 ppm to 33 ppm with minor decreases at 1.5 and 7 cmbsf. The Mn content fluctuates between 65.1 ppm and 92.5 ppm and the Fe content varies between 1.2 and 1.7 wt%.

In the sediments at the upper slope site (GC 5), the Al content varies between 1.4 and 1.7 wt%. The Mo content is lowest at the core top (1–2 ppm) and increases downcore to 7.3–7.5 ppm at the core bottom. The V content at this site increases from 26 ppm at the top of the core to 33.7 ppm at 13 cmbsf, then decreases to 26.8 ppm at 23 cmbsf. At site GC 5, Mn content ranges between 61.5 ppm and 78.5 ppm and Fe content ranges between 1.0 and 1.4 wt%.

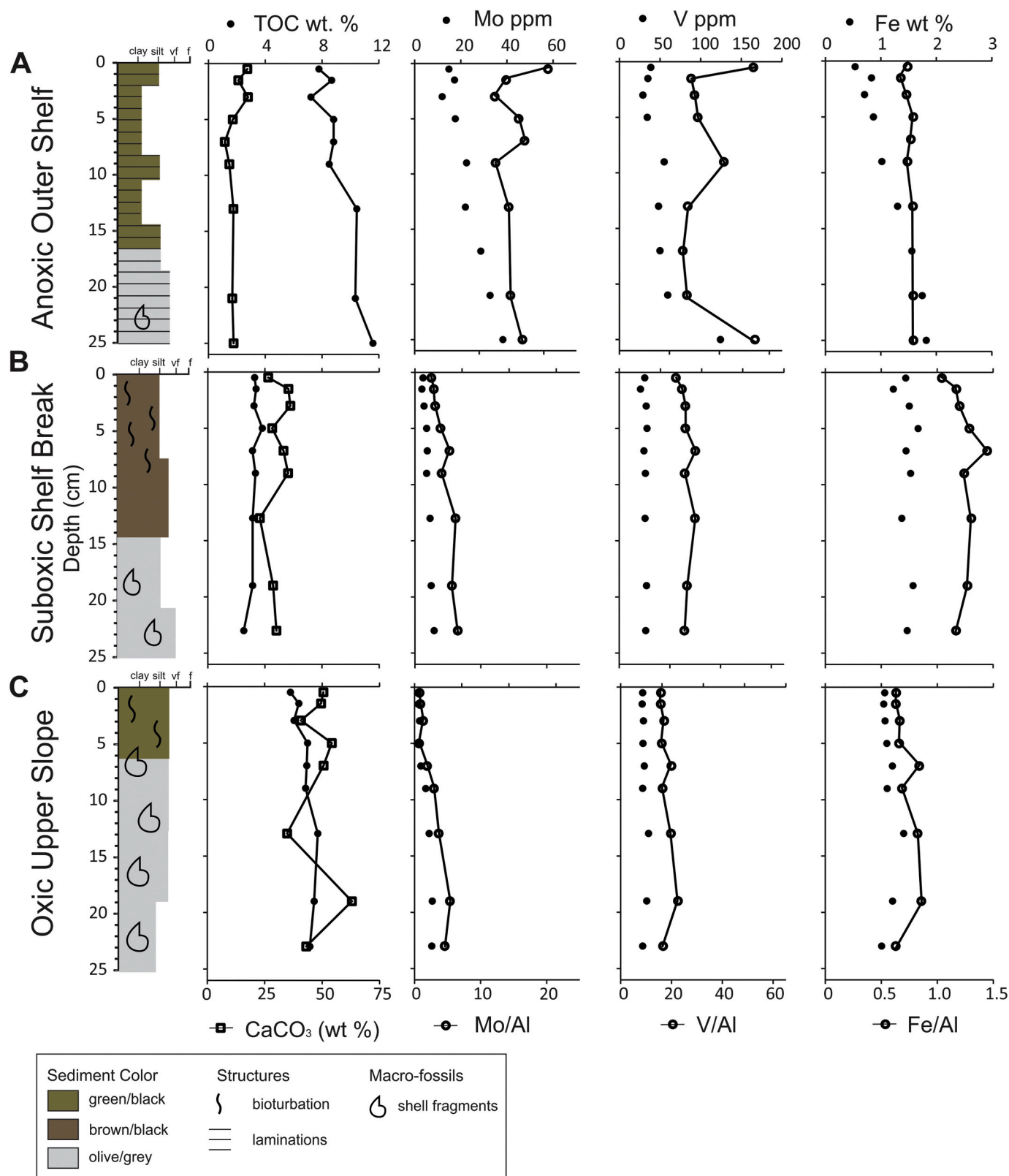


Fig. 3. Core descriptions, total organic carbon (TOC), and redox-sensitive trace metal content of sediment from the A. anoxic shelf (site 25020), B. suboxic shelf break (site GC 4), and C. oxidic upper slope (site GC 5). Trace metal/Aluminum (TM/Al) ratios are plotted alongside trace metal concentrations to normalize TM values against any lithogenic variation (e.g. Calvert and Pedersen, 1993). Trace metal measurements are represented by solid circles and TM/Al ratios are plotted as open circles with lines. Sedimentary core descriptions are from Cofrancesco (2016) and TOC data are from Abshire et al. (2020).

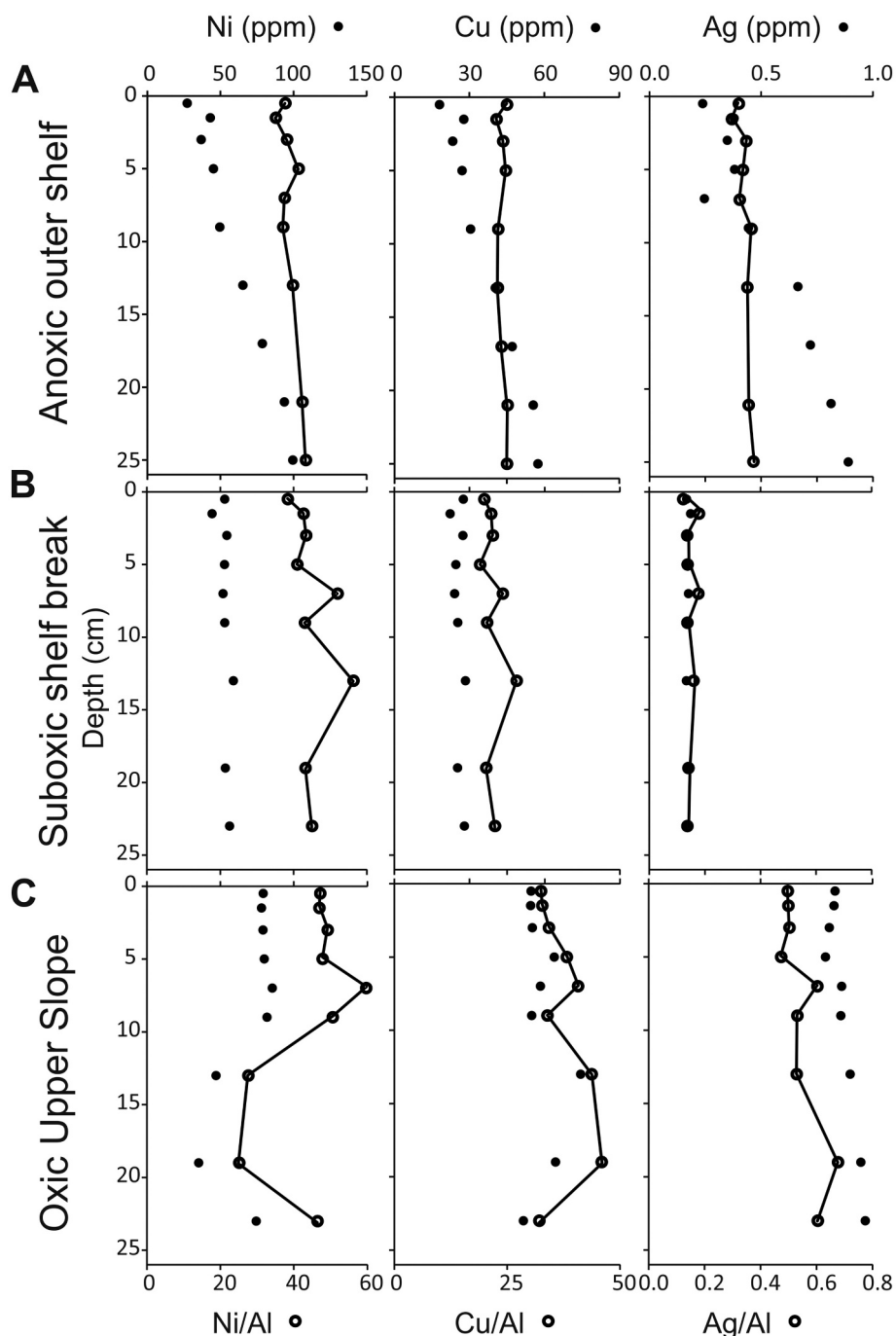


Fig. 4. Productivity-related solid-phase trace metal results from A) anoxic shelf (site 25020), B) suboxic shelf break (GC 4) and C) oxidic upper slope (GC 5). Metal concentrations are plotted with a solid black circle and TM/Al ratios are plotted as open circles with lines.

3.2.3. Ni, Cu and Ag

Solid-phase productivity-related trace metal data for sites 25020, GC 4, and GC 5 are shown in Fig. 4, and data are provided in the Appendix, Table A4. In the sediments from the shelf (site 25020), Ni contents are lowest (27.2 ppm) at the core top and increase with sediment depth to 99.5 ppm at 25 cmbsf with a slight peak to 43 ppm at 1.5 cm. The Cu content of the sediment from site 25020 shows a similar enrichment profile to Ni that increases downcore. Cu content at the top of the core is 18 ppm and reaches 57 ppm at 25 cmbsf. Like Ni, there is a minor increase in Cu content at 1.5 cmbsf. The Ag content at this site is 0.24 ppm in the uppermost sediment and increases slightly to 0.38 ppm at 1.5 cmbsf. Ag content decreases to 0.25 ppm at 7 cmbsf and increases steadily to 25 cmbsf where Ag content reaches 0.89 ppm.

At the shelf break (site GC 4), Ni content ranges between 51.9 ppm and 59 ppm, decreasing to 44.4 ppm at 1.5 cmbsf. Similarly, Cu content ranges between 22.3 ppm and 28.4 ppm with the lowest content (22.3 ppm) measured at 1.5 cmbsf. Ag content of shelf-break sediment is consistently between 0.17 ppm and 0.19 ppm throughout the core.

Sediment at the upper slope site (GC 5) contains between 78 and 80 ppm Ni in the upper 5 cm. Ni content increases to 85.4 ppm at 7 cmbsf then abruptly decreases to 35.2 ppm at 19 cmbsf. Ni content increases again to 74.4 ppm at 23 cmbsf. The Cu content of the uppermost 3 cm is between 54 ppm and 55 ppm and increases to 63.8 ppm at 5 cmbsf. Cu content then decreases to 54.8 ppm at 9 cmbsf and increases again to 74.3 ppm at 13 cmbsf. Cu content decreases once more to 54.4 ppm by 23 cmbsf. The Ag content of the upper slope sediment is

0.83 ppm at the top of the core and decreases slightly to 0.79 ppm. The Ag content increases to 0.97 ppm at 23 cmbsf.

4. Discussion

4.1. Shelf site 25020

Terrestrial input to the study area is low due to the absence of nearby perennial rivers in the area (Shannon and Nelson, 1996; Borchers et al., 2005) and measured Al contents of the shelf sediments are below 2.3 wt%. (as low as 0.7 wt%), thus trace metal enrichments are interpreted as having negligible detrital components. The sediments display geochemical characteristics of a reducing to highly-reducing environment. The low pore-water Fe (Fe_{PW}) concentration at the sediment-water interface (SWI) and slight ($\sim 0.09 \mu\text{M}$) increase in bottom water Fe are explained by the upward diffusion of reduced Fe (Canfield, 1989a; Severmann et al., 2010; Scholz et al., 2011), likely sourced from the apparent release of Fe from the solid-phase as a result of the reductive dissolution of Fe (oxyhydr)oxide minerals (e.g., Froelich et al., 1979; Canfield, 1989a) which appears to be occurring at a depth of 3 cmbsf and is indicated by increased Fe_{PW} at 3cmbsf (Fig. 2A). The observed downcore decrease in Fe_{PW} , along with the increase in solid-phase Mo, V, and Fe in the same interval suggests the presence of dissolved sulfide in the pore-waters (Berner, 1970; Raiswell and Canfield, 2012) and the likely subsequent formation of Fe sulfide minerals (e.g., pyrite) below 3 cmbsf. While there are no sulfide data available for this study, the sediments had a strong sulfide odor (see also Brüchert et al., 2003). A parallel core (GeoB-12,806, Goldhammer et al., 2011) measured dissolved sulfide in shelf sediment at 0–1 cmbsf. Furthermore, the dissolved sulfide concentration below 3 cm sediment depth must be greater than the threshold required for Mo to be scavenged from the pore-water as thiomolybdate (Helz et al., 1996; Erickson and Helz, 2000; Zheng et al., 2000; Poulson Brucker et al., 2009; Helz et al., 2011) and, consequently, to accumulate in the solid-phase (Fig. 3A, Table A4).

High productivity in surface waters above the shelf (Mollenhauer et al., 2002) is mirrored in the elevated concentration of organic carbon at this site (up to 11.6 wt%). The TOC, Ni, Cu, and Ag content all increase with depth indicating potentially periods of elevated productivity in the past. The Al content also increases with depth in the shelf sediments suggesting that the continental weathering, which contributed the Al, may have also delivered an increased amount of nutrients to the oceans, stimulating higher productivity (e.g. Jenkyns, 2010). Alternatively, the lower TOC and Al content in the upper portion of the core may be due to dilution by biosiliceous material (e.g. Borchers et al., 2005).

Previous studies have demonstrated, in modern shelf sediments, that the dominant source for trace metal accumulation is biogenic (Ni, Cu, and Ag) or related to seawater input (U and Mo) (Borchers et al., 2005). Since productivity-related metals are often incorporated into organic matter in the water column either by bioassimilation or adsorption (Brongersma-Sanders et al., 1980; Böning et al., 2015), and the redox-sensitive metals are enriched in the sediment, geochemical signals of the offshore Namibia shelf suggest a strong correlation between the accumulation of the organic material and the reducing conditions during deposition (Borchers et al., 2005).

4.2. Shelf break site GC 4

On the shelf break (site GC 4) suboxic bottom water (bottom water O_2 concentration of $1.11 \text{ mL L}^{-1} \text{ H}_2\text{O}$, Table 1, Abshire et al., 2020), high surface water productivity (Mollenhauer et al., 2002), and net erosion due to bottom currents (Mollenhauer et al., 2007) create a dynamic and unusual depositional environment. Erosion is the dominant control on organic matter deposition and outpaces accumulation at the shelf break site, resulting in the exposure of relatively old organic

carbon at the sediment surface (Mollenhauer et al., 2007; Abshire et al., 2020). The increased CaCO_3 content in the shelf break sediments, relative to the shelf sediments, is attributed to the observed shell fragments present in the core (Fig. 3B). Pore-waters contain a variable amount of Fe that fluctuates significantly with depth (Fig. 2B), indicating possible disturbances by burrowing organisms that were observed during core retrieval at the shelf break site (Fig. 3B). The benthic organisms are likely introducing slightly oxygenated bottom water ($1.11 \text{ mL O}_2 \text{ L}^{-1}$, Abshire et al., 2020) into the sediments through bio-irrigation (Aller, 1994; Kristensen, 2000), thus oxidizing the sediments, precipitating some Fe, and releasing V and Mo into the pore-water (Aller, 1994; Canfield, 1994).

Productivity proxy contents of Ni, Cu, and Ag, as well as TOC contents, are all comparatively lower in the shelf break sediments, versus the shelf site, and concentrations of these metals remain consistent throughout the sediment column (Fig. 4B). The lower productivity-related metal content may be related to the known significant erosion, but may also indicate an overall smaller contribution of organic matter from surface productivity in this location through time. Solid-phase redox-sensitive TMs Mo and V both show slight enrichments in the shelf break sediments and the highest Fe contents of all three locations; further evidence of the introduction of oxygenated waters into the sediments, allowing for the precipitation of Fe (Canfield, 1994). The Mo data are consistent with a previous study that reported high U content (39–50 ppm), relative to TOC, in the shelf break sediment (Abshire et al., 2020), documenting a range of uranium isotope ($^{234}\text{U}/^{238}\text{U}$) values in NCM shelf break sediment that approached secular equilibrium. This implies that the shelf break sediment is significantly older than sediment from the outer shelf and upper slope of the NCM – a result of the erosional regime that dominates the shelf break (Mollenhauer et al., 2007) and the subsequent exposure of recalcitrant organic material to suboxic conditions. The erosional regime under low-oxygen conditions may also be responsible for Mo enrichment, relative to TOC content, in the shelf break sediments. While recent work has found a generally strong correlation between TOC and major redox-sensitive trace metals in many shales (Algeo and Liu, 2020), the decoupling of TOC and redox-sensitive trace metals (such as Mo and U) has been observed in the geologic record (e.g., Lüning and Kolonic, 2003; Scott et al., 2017). The erosional exposure of recalcitrant organic matter that is occurring on the NCM shelf break may provide an alternative explanation to late diagenetic or catagenetic carbon loss in shales with pronounced decoupling of redox-sensitive TMs and TOC.

4.3. Upper slope site GC 5

In sediments at site GC 5 on the upper slope, the absence of laminations and the direct CTD measurements of dissolved oxygen in the bottom water (O_2 concentration of $3.36 \text{ mL L}^{-1} \text{ H}_2\text{O}$, Table 1, Abshire et al., 2020) place the depositional conditions under oxic conditions. The upper slope sediments show relatively high CaCO_3 content (40–63 wt%, Table A3) relative to the shelf and shelf break, which is attributed to the shell fragments within the sediments (Fig. 3C). Low solid-phase Mo and V content (Fig. 3C, Table A4), as well as the lowest EFs of all of the studied sites (Mo EF < 14, and V EF = 1, Table A5) represent diagenetic pathways that include oxic respiration. Interestingly, TOC contents are high (up to 7.7 wt%), considering organic carbon is assumed to not usually be well-preserved under oxic conditions (Demaison and Moore, 1980; Tyson, 1987; Canfield, 1989b; Piper and Calvert, 2009). Reducing conditions below the SWI are indicated by an increase in Fe_{PW} (up to $16 \mu\text{M}$), likely due to the reduction of Fe-oxides (Fig. 2C). The followed observed decrease in Fe_{PW} may be related to the presence of dissolved sulfides at depth which, however, likely did not exceed concentrations needed for Mo(IV) precipitation (Helz et al., 1996; Erickson and Helz, 2000; Poulson Brucker et al., 2009; Helz et al., 2011) as solid-phase Mo enrichments are very minor (Fig. 3C). Dissolved sulfide in nearby sediments did not contain

dissolved sulfide above 50 cmbsf (core GeoB-12,802, Goldhammer et al., 2011). While the solid-phase Mo content in the upper slope sediments is low, dissolved Mo accumulates in the pore-water with Mo_{PW} reaching concentrations up to nearly 3000 nM (Fig. 2C). The Mo_{PW} profile indicates upward diffusion of Mo with a source in the deeper sediments. Such a deep Mo source could suggest higher Mo accumulation in the past when, during the last glacial maximum (LGM), the upwelling cells offshore Namibia moved further offshore and TOC accumulation on the slope was 84% higher than it is today (Mollenhauer et al., 2002). However, based on core-top ages of nearby cores and local sedimentation rates, it is unlikely that the LGM is recorded in the surface sediments sampled for this study.

Elevated quantities of productivity proxy elements Ni, Cu, and Ag at the upper slope site (Fig. 4C) suggest that the high TOC content of the upper slope sediments is related to high productivity in the water column. However, it has been previously shown that the source of the bulk of the organic carbon on the upper slope is the NCM shelf, and that direct input from surface waters does not contribute significantly to the particle flux at depth (Giraudeau et al., 2000). The increased concentrations of productivity-related metals in the sediments at the upper slope site do not positively correspond to enrichments of redox-sensitive trace metals as seen on the shelf. Lateral transport of organic-rich sediment from the anoxic shelf on the NCM (Inthorn et al., 2006a, 2006b; Mollenhauer et al., 2007) is likely responsible for enrichments of Ni, Cu, and Ag in the upper slope sediments (average EFs = 5, 7, and 62, respectively, Table A5). In contrast to the shelf and shelf break sites in this study, Cu does not behave similarly to Ni at the upper slope site. Instead, Cu and also Ag show larger enrichments than Ni, relative to the shelf site, suggesting that some Ni may be lost during the partial remineralization of the organic matter (e.g. Moore et al., 1988), during vertical transport through oxic water below the OMZ. Alternatively, Cu and Ag might be more efficiently scavenged from the water column by particulate organics and/or Fe–Mn (oxyhydr)oxides during transport (e.g. Little et al., 2015). The Ag content of the NCM upper slope sediment is exceptionally high, with Ag reaching up to 0.97 ppm (Fig. 4C) when compared to the average shale Ag content of ~0.07 ppm (Turekian and Wedepohl, 1961; Table A1). Our data suggest that observations of NCM sediments are similar to those from the Northwestern United States Continental Margin (Morford et al., 2008), Peruvian Margin (Böning et al., 2004), Central Chilean Margin, and Western Canadian Margin (McKay and Pedersen, 2008) where Ag is scavenged by sinking particles, especially within OMZs, resulting in a greater flux of solid-phase Ag to the sediment under a deeper water column (Böning et al., 2004; McKay and Pedersen, 2008; Morford et al., 2008).

4.4. Effects of redeposition on geochemical signals

Offshore sediment transport along the NCM results in the release of some redox-sensitive trace metals as sediments are settling through an oxygenated water column; a process that is reflected in the preserved geochemical properties of the redepositional zone (Fig. 5). Upon redeposition on the upper slope, the partially-remineralized organic matter remains, retaining the productivity-related trace metal signal (Ni, Cu, and Ag) despite oxic conditions. Redox-sensitive elements Mo and V are highly influenced by water column conditions and thus deviations in their abundance occur through redeposition. Because enrichments of Ni, Cu, and Ag are primarily controlled by their association with organic matter in the absence of dissolved sulfides (Ni and Cu, Tribouillard et al., 2006; Ag, McKay and Pedersen, 2008), the enrichments of productivity-related TM in the upper slope sediment suggest (a) resistance of these metals to dissolution during offshore transport, and (b) the addition of a smaller amount of fresh organic matter from the productive water column above the upper slope. All of the geochemical and sedimentological signals observed in the NCM upper slope sediments – bioturbation, high organic carbon contents, enrichments in

productivity proxy metals, and depletion in the redox-sensitive metals (when compared to the average shale, Turekian and Wedepohl, 1961) – characterize the sediments of the redepositional site. Such a distinct geochemical signature, when found in ancient rock, could be used to identify a paleo-redepositional setting from beneath an upwelling OMZ especially when considering the global location of the setting (i.e. eastern margins of the ocean basin).

5. Summary and conclusions

Lateral transport of organic-rich sediments resulted in highly varied geochemical signals along the NCM. Through these observations, we can define the geochemical and sedimentary properties of a redepositional zone, which will be significant for paleoceanographic studies. The redepositional area at the upper slope on the NCM is characterized by bioturbated, organic-rich (> 5 wt%) sediments with relatively low Mo contents compared to the shelf and shelf break, no significant enrichments of Fe and V, substantial enrichments of Ni, Cu, and especially high Ag content (Fig. 5).

While Ag is a useful paleoproductivity proxy, it is coupled to the water column depth. Similar to Ba, Ag is best applied to sediments deposited at great water depths. Moreover, Ag scavenging seems to be dependent on the amount of Ag available in the water column (e.g., Flegal et al., 1995), which may vary with different ocean settings (and thus likely with overall water column mixing). Unlike Barium, which is subject to remobilization from marine sediments during diagenesis (e.g., McManus et al., 1994; Torres et al., 1996; Riedinger et al., 2006), the consistent Ag concentration throughout the NCM sediment columns suggests that Ag may be more resistant to diagenetic alteration. We thereby postulate that Ag can provide, in addition to its application to paleoproductivity reconstruction, information about water depth and water mixing properties, when applied in combination with other paleo proxies.

While not all ocean upwelling systems undergo intense lateral redeposition processes to the extent of the modern NCM, and the single offshore transect from shelf to slope represents a small cross-section of a large upwelling area, this study provides a step toward a more complete understanding of the sedimentary controls on geochemical signals in organic carbon-rich sediments. Our data suggest that the distinct multiproxy geochemical signatures observed in the offshore transect around 25°S could be a tool for identifying redepositional environments below ancient OMZs. This observation could potentially help constrain some of the difficulties interpreting organic-rich shales that display evidence of benthic life, such as the Jurassic Kimmeridge Clay (e.g. Wignall and Myers, 1988) and the Jurassic Posidonia Shale (e.g. Röhl et al., 2001) and may have various redox conditions throughout the basin both spatially and through time. Due to the expansion of OMZs in the past several decades, and predictions of continued ocean deoxygenation (Stramma et al., 2008; Schmidtke et al., 2017), understanding how proxy metals are incorporated into sediment under a variety of depositional conditions is critical to the interpretation of past OAEs and predictions of future changes to ocean oxygenation.

Declaration of Competing Interest

The authors declare that they have no known competing financial interests or personal relationships that could have appeared to influence the work reported in this paper.

Acknowledgements

This manuscript is based upon work supported by the National Science Foundation (NSF) Graduate Research Fellowship Program under Grant No. 1746055. Any opinions, findings, and conclusions or recommendations expressed in this manuscript are those of the authors

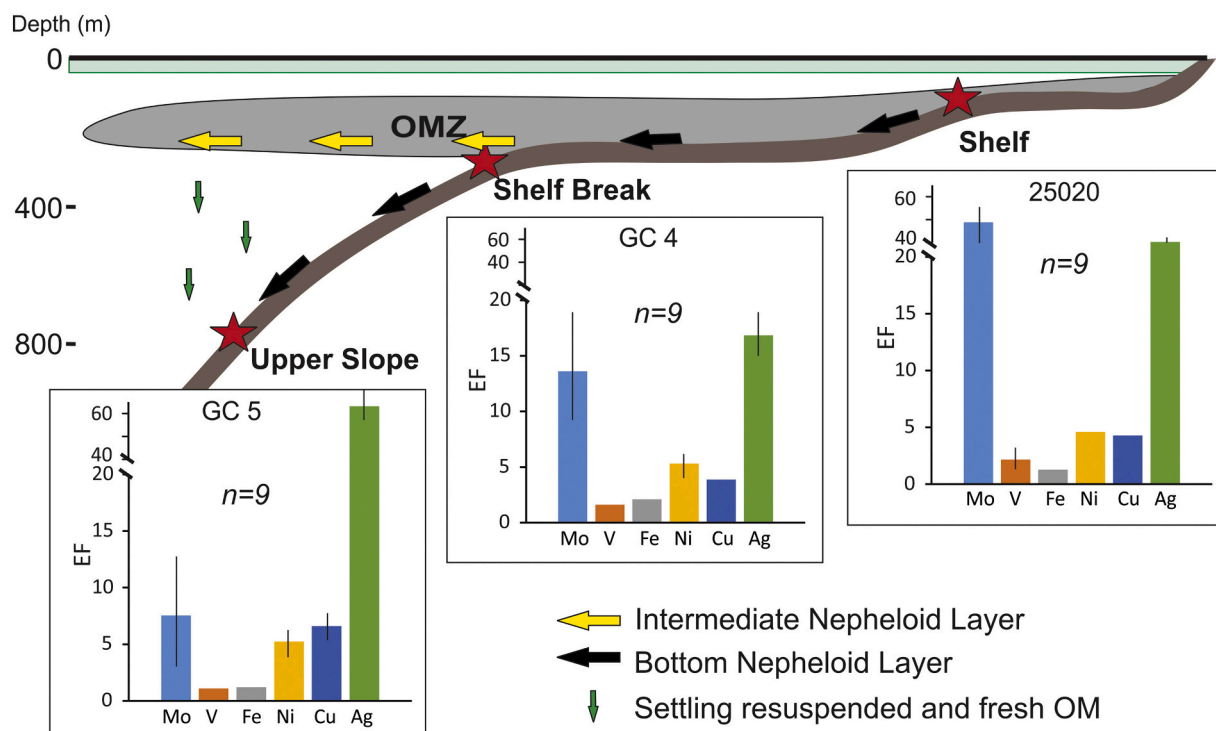


Fig. 5. Conceptual model showing the direction of sediment transport in intermediate (yellow arrows) and bottom (black arrows) nepheloid layers, settling of suspended and fresh organic matter (green arrows), the position of the OMZ, and the enrichment factors (EF) of solid-phase elements Mo, V, Fe, Ni, Cu, and Ag at each sample site (red stars, modified after Abshire et al., 2020). Black vertical lines on bar graphs show the standard deviation of each EFs, *n* gives the number of analyses. (For interpretation of the references to color in this figure legend, the reader is referred to the web version of this article).

and do not necessarily reflect the views of the National Science Foundation. Grants to JDO (NSF OCE and NASA Exobiology) helped to fund the FSU and National High Magnetic Field Laboratory (DMR-1157490) analysis. The authors thank the Regional Graduate Network in Oceanography program, the Research Discovery Camp, and the crew of the Research Vessel Mirabilis. We gratefully acknowledge T. Wu for

help and assistance in the lab, C. Scott, J. Donoghue, J. Puckette, and G. Cook for helpful conversation and insight, C. März for comments on a previous version, T. Algeo, and anonymous reviewers for their constructive comments which greatly improved the manuscript, and Adina Paytan for editorial handling. This is an Oklahoma State University - Boone Pickens School of Geology contribution # 2020-116.

Appendix A

Table A1
The average shale content of selected elements from Turekian and Wedepohl (1961).

| Element | Avg. Shale Content (ppm) |
|-----------------|--------------------------|
| Aluminum (Al) | 80,000 |
| Manganese (Mn) | 850 |
| Vanadium (V) | 130 |
| Iron (Fe) | 47,200 |
| Nickel (Ni) | 68 |
| Copper (Cu) | 45 |
| Molybdenum (Mo) | 2.6 |
| Silver (Ag) | 0.07 |

Table A2
Bottom water (BW) and pore-water concentrations of Fe, Mo and V from the shelf (25020), shelf break (GC 4), and upper slope (GC 5).

| Sample | Depth | V | Fe | Mo | Mn |
|-------------|-------|--------|-------|--------|------|
| Name | cm | nM | µM | nM | µM |
| 25020-BW-51 | 0 | 19.84 | 0.15 | 114.03 | 0.00 |
| 25020-BW-52 | 0 | 16.18 | 0.25 | 107.69 | 0.00 |
| 25020-1-53 | 0.5 | 117.30 | 0.16 | 119.52 | 0.01 |
| 25020-3-54 | 1.5 | 39.11 | 3.40 | 39.56 | 0.06 |
| 25020-5-55 | 3 | 38.29 | 10.48 | 22.29 | 0.13 |

(continued on next page)

Table A2 (continued)

| Sample | Depth | V | Fe | Mo | Mn |
|---------------|-------|--------|-------|---------|------|
| Name | cm | nM | μM | nM | μM |
| 25020-7-56 | 5 | 50.97 | 2.53 | 25.19 | 0.15 |
| 25020-9-57 | 7 | 24.99 | 0.23 | 20.74 | 0.01 |
| 25020-11-58 | 9 | 16.55 | 0.23 | 13.25 | 0.04 |
| 25020-13-59 | 13 | 35.34 | 1.44 | 0.91 | 0.10 |
| 25020-15-60 | 17 | 25.25 | 0.63 | 5.04 | 0.05 |
| 25020-19-61 | 21 | 64.59 | 0.38 | 150.59 | 0.05 |
| 25020-21-62 | 25 | 664.25 | 0.20 | 106.43 | 0.02 |
| GeoChe4-BW-63 | 0 | 39.93 | 0.22 | 106.32 | 0.00 |
| GeoChe4-BW-64 | 0 | 38.25 | 0.15 | 111.52 | 0.00 |
| GeoChe4-1-65 | 0.5 | 49.78 | 4.24 | 157.49 | 0.01 |
| GeoChe4-3-66 | 1.5 | 53.73 | 8.49 | 189.91 | 0.01 |
| GeoChe4-5-67 | 3 | 22.05 | 6.12 | 194.51 | 0.03 |
| GeoChe4-7-68 | 5 | 57.77 | 2.31 | 291.68 | 0.03 |
| GeoChe4-9-69 | 7 | 53.99 | 4.64 | 246.35 | 0.02 |
| GeoChe4-11-70 | 9 | 44.31 | 8.83 | 144.83 | 0.14 |
| GeoChe4-15-71 | 13 | 72.37 | 5.85 | 408.90 | 0.09 |
| GeoChe4-19-72 | 19 | 127.21 | 15.87 | 1883.61 | 0.58 |
| GeoChe4-21-73 | 21 | 102.85 | 0.17 | 2208.17 | 0.01 |
| GeoChe5-BW-74 | 0 | 47.43 | 0.00 | 123.45 | 0.00 |
| GeoChe5-BW-75 | 0 | 44.31 | 0.00 | 103.80 | 0.00 |
| GeoChe5-1-76 | 0.5 | 44.74 | 4.51 | 345.18 | 0.05 |
| GeoChe5-3-77 | 1.5 | 76.85 | 3.96 | 692.99 | 0.02 |
| GeoChe5-5-78 | 3 | 64.90 | 5.65 | 441.91 | 0.06 |
| GeoChe5-7-79 | 5 | 37.94 | 15.28 | 384.78 | 0.11 |
| GeoChe5-9-80 | 7 | 47.43 | 16.13 | 562.34 | 0.21 |
| GeoChe5-11-81 | 9 | 25.41 | 6.20 | 800.55 | 0.15 |
| GeoChe5-15-82 | 13 | 72.06 | 0.04 | 1560.65 | 0.06 |
| GeoChe5-19-83 | 19 | 83.18 | 0.00 | 2236.06 | 0.05 |
| GeoChe5-21-84 | 21 | 77.94 | 0.00 | 3033.26 | 0.03 |
| NIST 1643f | | 661.0 | 0.78 | 1134.0 | 0.62 |

Table A3

Measured TOC* and CaCO₃ content of sediments from the shelf (25020), shelf break (GC 4), and upper slope (GC 5).

| Sample Name | Depth cm | TOC* wt% | CaCO ₃ wt% |
|-------------|----------|----------|-----------------------|
| 25020-11 | 0.5 | 7.8 | 17.1 |
| 25020-12 | 1.5 | 8.7 | 13.2 |
| 25020-13 | 3 | 7.2 | 17.4 |
| 25020-14 | 5 | 8.8 | 10.8 |
| 25020-15 | 7 | 8.8 | 7.2 |
| 25020-16 | 9 | 8.5 | 9.2 |
| 25020-17 | 13 | 10.4 | 11.0 |
| 25020-18 | – | – | – |
| 25020-19 | 21 | 10.3 | 10.5 |
| 25020-20 | 25 | 11.6 | 11.1 |
| GC 4-21 | 0.5 | 3.3 | 26.4 |
| GC 4-22 | 1.5 | 3.4 | 35.2 |
| GC 4-23 | 3 | 3.2 | 36.1 |
| GC 4-24 | 5 | 3.8 | 28.1 |
| GC 4-25 | 7 | 3.1 | 33.1 |
| GC 4-26 | 9 | 3.3 | 35.2 |
| GC 4-27 | 13 | 3.1 | 22.8 |
| GC 4-28 | 19 | 3.1 | 28.6 |
| GC 4-29 | 23 | 2.5 | 30.0 |
| GC 5-30 | 0.5 | 5.8 | 50.5 |
| GC 5-31 | 1.5 | 6.4 | 49.5 |
| GC 5-32 | 3 | 6.0 | 40.8 |
| GC 5-33 | 5 | 7.0 | 54.2 |
| GC 5-34 | 7 | 6.9 | 50.6 |
| GC 5-35 | 9 | 6.8 | – |
| GC 5-36 | 13 | 7.7 | 34.8 |
| GC 5-37 | 19 | 7.4 | 63.0 |
| GC 5-38 | 23 | 7.1 | 43.1 |

– Indicates no measurement collected

*TOC data from sites 25020, GC 4 and GC 5 were previously reported in [Abshire et al. \(2020\)](#).

Table A4

Solid-phase major and trace element content of sediments from the shelf (25020), shelf break (GC 4), and upper slope (GC 5).

| Sample Name | Depth cm | Al wt% | V ppm | Mn ppm | Fe wt% | Ni ppm | Cu ppm | Mo ppm | Ag ppm |
|-------------|----------|--------|--------|---------|--------|--------|--------|--------|--------|
| 25020-11 | 0.5 | 0.72 | 38.55 | 38.03 | 0.53 | 27.17 | 18.03 | 14.85 | 0.24 |
| 25020-12 | 1.5 | 1.22 | 35.00 | 56.46 | 0.83 | 42.93 | 27.76 | 17.29 | 0.38 |
| 25020-13 | 3 | 0.96 | 28.93 | 61.41 | 0.70 | 36.84 | 23.32 | 11.94 | 0.35 |
| 25020-14 | 5 | 1.09 | 34.22 | 62.59 | 0.86 | 45.21 | 27.08 | 17.58 | 0.38 |
| 25020-15 | 7 | – | – | 60.84 | – | – | – | – | 0.25 |
| 25020-16 | 9 | 1.32 | 55.12 | – | 1.02 | 49.57 | 30.47 | 22.46 | 0.44 |
| 25020-17 | 13 | 1.76 | 48.11 | 86.52 | 1.30 | 65.36 | 40.40 | 22.01 | 0.66 |
| 25020-18 | 17 | 1.97 | 50.02 | – | 1.56 | 78.56 | 47.08 | 28.69 | 0.72 |
| 25020-19 | 21 | 2.20 | 59.50 | 93.40 | 1.74 | 93.63 | 55.54 | 32.70 | 0.81 |
| 25020-20 | 25 | 2.29 | 124.34 | 159.74 | 1.82 | 99.49 | 57.41 | 38.24 | 0.89 |
| GC4-21 | 0.5 | 1.38 | 30.78 | 82.47 | 1.44 | 53.03 | 27.54 | 3.43 | 0.17 |
| GC4-22 | 1.5 | 1.04 | 25.63 | 65.10 | 1.22 | 44.40 | 22.29 | 2.96 | 0.19 |
| GC4-23 | 3 | 1.25 | 32.58 | 88.07 | 1.50 | 54.45 | 27.33 | 3.84 | 0.17 |
| GC4-24 | 5 | 1.29 | 33.58 | 92.49 | 1.66 | 52.87 | 24.52 | 5.00 | 0.18 |
| GC4-25 | 7 | 1.00 | 29.88 | 72.63 | 1.44 | 51.94 | 24.02 | 5.22 | 0.18 |
| GC4-26 | 9 | 1.23 | 31.65 | 82.75 | 1.53 | 53.02 | 25.26 | 4.97 | 0.17 |
| GC4-27 | 13 | 1.05 | 31.26 | 76.78 | 1.37 | 59.03 | 28.38 | 6.45 | 0.17 |
| GC4-28 | 19 | 1.24 | 32.95 | 80.33 | 1.57 | 53.51 | 25.18 | 6.92 | 0.17 |
| GC4-29 | 23 | 1.25 | 32.10 | 81.81 | 1.46 | 56.43 | 27.95 | 8.14 | 0.17 |
| GC5-30 | 0.5 | 1.68 | 26.61 | 66.13 | 1.06 | 79.23 | 54.47 | 1.28 | 0.83 |
| GC5-31 | 1.5 | 1.66 | 26.16 | 65.82 | 1.04 | 77.97 | 54.35 | 1.48 | 0.83 |
| GC5-32 | 3 | 1.60 | 27.58 | 67.41 | 1.07 | 79.03 | 54.98 | 2.11 | 0.81 |
| GC5-33 | 5 | 1.67 | 27.04 | 68.70 | 1.10 | 79.92 | 63.79 | 1.16 | 0.79 |
| GC5-34 | 7 | 1.43 | 28.55 | 72.78 | 1.20 | 85.40 | 58.21 | 2.72 | 0.86 |
| GC5-35 | 9 | 1.62 | 26.70 | 67.95 | 1.11 | 81.80 | 54.78 | 4.74 | 0.86 |
| GC5-36 | 13 | 1.70 | 33.70 | 78.50 | 1.40 | 47.00 | 74.30 | 6.20 | 0.90 |
| GC5-37 | 19 | 1.40 | 31.60 | 66.80 | 1.20 | 35.20 | 64.30 | 7.50 | 0.95 |
| GC5-38 | 23 | 1.60 | 26.75 | 61.52 | 1.01 | 74.44 | 51.41 | 7.33 | 0.97 |
| NIST 2702 | | 7.92 | 331.85 | 1737.75 | 7.31 | 69.81 | 102.76 | 10.04 | 0.68 |
| SCO-1 | | 6.83 | 125.77 | 390.89 | 3.47 | 25.00 | 25.86 | 0.85 | – |
| SDO-1 | | 6.20 | 146.47 | 308.33 | 6.02 | 89.82 | 50.33 | 158.27 | – |

– Indicates no measurement collected.

Table A5

Calculated enrichment factors (EFs) for all sample locations.

| Sample Name | Mo EF | V EF | Fe EF | Ni EF | Cu EF | Ag EF |
|-------------|-------|------|-------|-------|-------|-------|
| 25020-11 | 64 | 3 | 1 | 4 | 4 | 38 |
| 25020-12 | 44 | 2 | 1 | 4 | 4 | 35 |
| 25020-13 | 38 | 2 | 1 | 4 | 4 | 41 |
| 25020-14 | 50 | 2 | 1 | 5 | 4 | 40 |
| 25020-15 | – | – | – | – | – | – |
| 25020-16 | 52 | 3 | 1 | 4 | 4 | 38 |
| 25020-17 | 39 | 2 | 1 | 4 | 4 | 43 |
| 25020-18 | 45 | 2 | 1 | 5 | 4 | 42 |
| 25020-19 | 46 | 2 | 1 | 5 | 4 | 42 |
| 25020-20 | 51 | 3 | 1 | 5 | 4 | 44 |
| GC 4-21 | 8 | 1 | 2 | 5 | 4 | 14 |
| GC 4-22 | 9 | 2 | 2 | 5 | 4 | 20 |
| GC 4-23 | 9 | 2 | 2 | 5 | 4 | 16 |
| GC 4-24 | 12 | 2 | 2 | 5 | 3 | 16 |
| GC 4-25 | 16 | 2 | 2 | 6 | 4 | 20 |
| GC 4-26 | 12 | 2 | 2 | 5 | 4 | 16 |
| GC 4-27 | 19 | 2 | 2 | 7 | 5 | 18 |
| GC 4-28 | 17 | 2 | 2 | 5 | 4 | 16 |
| GC 4-29 | 20 | 2 | 2 | 5 | 4 | 16 |
| GC 5-30 | 2 | 1 | 1 | 6 | 6 | 57 |
| GC 5-31 | 3 | 1 | 1 | 6 | 6 | 57 |
| GC 5-32 | 4 | 1 | 1 | 6 | 6 | 57 |
| GC 5-33 | 2 | 1 | 1 | 6 | 7 | 54 |
| GC 5-34 | 6 | 1 | 1 | 7 | 7 | 69 |
| GC 5-35 | 9 | 1 | 1 | 6 | 6 | 61 |
| GC 5-36 | 11 | 1 | 1 | 3 | 8 | 61 |
| GC 5-37 | 16 | 1 | 1 | 3 | 8 | 77 |
| GC 5-38 | 14 | 1 | 1 | 5 | 6 | 69 |

– Indicates EF not calculated.

References

- Abshire, M.L., Romaniello, S.J., Kuzminov, A.M., Cofrancesco, J., Severmann, S., Riedinger, N., 2020. Uranium isotopes as a proxy for primary depositional redox conditions in organic-rich marine systems. *Earth Planet. Sci. Lett.* 529, 115878.
- Algeo, T., Liu, J., 2020. A re-assessment of elemental proxies for paleoredox analysis. *Chemical Geology* 540 (119549). <https://doi.org/10.1016/j.chemgeo.2020.119549>.
- Algeo, T., Lyons, T., 2006. Mo–total organic carbon covariation in modern anoxic marine environments: Implications for analysis of paleoredox and paleohydrographic conditions. *Paleoceanography* 21 (1). <https://doi.org/10.1029/2004PA001112>.
- Algeo, T., Maynard, J., 2004. Trace-element behavior and redox facies in core shales of Upper Pennsylvanian Kansas-type cyclothems. *Chem. Geol.* 206 (3), 289–318. <https://doi.org/10.1016/j.chemgeo.2003.12.009>.
- Algeo, T., Rowe, H., 2012. Paleoceanographic applications of trace-metal concentration data. *Chem. Geol.* 324, 6–18. <https://doi.org/10.1016/j.chemgeo.2011.09.002>.
- Aller, R.C., 1994. Bioturbation and remineralization of sedimentary organic matter: effects of redox oscillation. *Chem. Geol.* 114 (3–4), 331–345.
- Bennett, W., Canfield, D., 2020. Redox-sensitive trace metals as paleoredox proxies: A review and analysis of data from modern sediments. *Earth-Science Reviews* 204 (103175). <https://doi.org/10.1016/j.earscirev.2020.103175>.
- Berger, W., Wefer, G., 2002. On the reconstruction of upwelling history: Namibia upwelling in context. *Mar. Geol.* 180 (1), 3–28. [https://doi.org/10.1016/S0025-3227\(01\)00203-1](https://doi.org/10.1016/S0025-3227(01)00203-1).
- Berner, R., 1970. Sedimentary pyrite formation. *Am. J. Sci.* 268 (1), 1–23.
- Böning, P., Brumsack, H.-J., Böttcher, M.E., Schnetger, B., Kriete, C., Kallmeyer, J., Borchers, S.V., 2004. Geochemistry of Peruvian near-surface sediments. *Geochim. Cosmochim. Acta* 68, 4429–4451. <https://doi.org/10.1016/j.gca.2004.04.027>.
- Böning, P., Cuypers, S., Grunwald, M., Schnetger, B., Brumsack, H.-J., 2005. Geochemical characteristics of Chilean upwelling sediments at ~36° S. *Mar. Geol.* 220 (1–4), 1–21. <https://doi.org/10.1016/j.margeo.2005.07.005>.
- Böning, P., Schnetger, B., Belz, L., Ferdelman, T., Brumsack, H.-J., Pahnke, K., 2020. Sedimentary iron cycling in the Benguela upwelling system off Namibia. *Earth and Planetary Science Letters* 538 (116212). <https://doi.org/10.1016/j.epsl.2020.116212>.
- Böning, P., Shaw, T., Pahnke, K., Brumsack, H.-J., 2015. Nickel as indicator of fresh organic matter in upwelling sediments. *Geochim. Cosmochim. Acta* 162, 99–108. <https://doi.org/10.1016/j.gca.2015.04.027>.
- Borchers, S., Schnetger, B., Böning, P., Brumsack, H., 2005. Geochemical signatures of the Namibian diatom belt: Perennial upwelling and intermittent anoxia. *Geochim. Geophys. Geosyst.* 6 (6). <https://doi.org/10.1029/2004GC000886>.
- Breit, G.N., Wanty, R.B., 1991. Vanadium accumulation in carbonaceous rocks – a review of geochemical controls during deposition and diagenesis. *Chem. Geol.* 91 (2), 83–97. [https://doi.org/10.1016/0009-2541\(91\)90083-4](https://doi.org/10.1016/0009-2541(91)90083-4).
- Bremner, J.M., 1983. Biogenic sediments on the South West African (Namibian) continental margin. In: Thiede, J., Suess, E. (Eds.), *Coastal Upwelling, its Sediment Record, Part B: Sedimentary Records of Ancient Coastal Upwelling*. Plenum, New York, pp. 73–103.
- Bremner, J.M., Willis, J.P., 1993. Mineralogy and geochemistry of the clay fraction of sediments from the Namibian continental margin and the adjacent hinterland. *Mar. Geol.* 115, 85–116. [https://doi.org/10.1016/0025-3227\(93\)90076-8](https://doi.org/10.1016/0025-3227(93)90076-8).
- Brongersma-Sanders, M., Stephan, K., Kwee, T., De Bruin, M., 1980. Distribution of minor elements in cores from the Southwest Africa shelf with notes on plankton and fish mortality. *Mar. Geol.* 37 (1–2), 91–132. [https://doi.org/10.1016/0025-3227\(80\)90013-4](https://doi.org/10.1016/0025-3227(80)90013-4).
- Brüchert, V., Jørgensen, B.B., Neumann, K., Riechmann, D., Schlösser, M., Schulz, H., 2003. Regulation of bacterial sulfate reduction and hydrogen sulfide fluxes in the central Namibian coastal upwelling zone. *Geochim. Cosmochim. Acta* 67 (23), 4505–4518. [https://doi.org/10.1016/S0016-7037\(03\)00275-8](https://doi.org/10.1016/S0016-7037(03)00275-8).
- Bruland, K.W., 1983. Trace elements in seawater. In: Riley, J.P., Chester, R. (Eds.), *Chemical Oceanography*, vol. 8. Elsevier, New York, pp. 158–220.
- Bruland, K.W., Lohan, M.C., 2006. Controls of trace metals in seawater. *Oceans Marine Geochem.* 6, 23–47.
- Brumsack, H.-J., 1989. Geochemistry of recent TOC-rich sediments from the Gulf of California and the Black Sea. *Geol. Rundsch.* 78 (3), 851–882.
- Brumsack, H.-J., 2006. The trace metal content of recent organic carbon-rich sediments: implications for cretaceous black shale formation. *Palaeogeogr. Palaeoclimatol. Palaeoecol.* 232 (2), 344–361. <https://doi.org/10.1016/j.palaeo.2005.05.011>.
- Calvert, S.E., Pedersen, T.F., 1993. Geochemistry of recent oxic and anoxic marine sediments: Implications for the geological record. In: Parkes, R.J., Westbroek, P., de Leeuw, J.W. (Eds.), *Marine Sediments, Burial, Pore Water Chemistry, Microbiology and Diagenesis*. Marine Geology. 113. pp. 67–88. [https://doi.org/10.1016/0025-3227\(93\)90150-T](https://doi.org/10.1016/0025-3227(93)90150-T).
- Calvert, S.E., Piper, D.Z., 1984. Geochemistry of ferromanganese nodules from DOMES Site a, Northern Equatorial Pacific: Multiple diagenetic metal sources in the deep sea. *Geochim. Cosmochim. Acta* 48 (10), 1913–1928.
- Canfield, D.E., 1989a. Reactive iron in marine sediments. *Geochim. Cosmochim. Acta* 53, 619–632. [https://doi.org/10.1016/0016-7037\(89\)90005-7](https://doi.org/10.1016/0016-7037(89)90005-7).
- Canfield, D.E., 1989b. Sulfate reduction and oxic respiration in marine sediments: implications for organic carbon preservation in euxinic environments. *Deep-Sea Res.* 36, 121–138. [https://doi.org/10.1016/0198-0149\(89\)90022-8](https://doi.org/10.1016/0198-0149(89)90022-8).
- Canfield, D.E., 1994. Factors influencing organic carbon preservation in marine sediments. *Chem. Geol.* 114 (3), 315–329.
- Carr, M.E., 2001. Estimation of potential productivity in Eastern Boundary Currents using remote sensing. *Deep Sea Research Part II: Topical Studies in Oceanography* 49, 59–80. [https://doi.org/10.1016/S0967-0645\(01\)00094-7](https://doi.org/10.1016/S0967-0645(01)00094-7).
- Chang, A.S., Pichevin, L., Pedersen, T.F., Gray, V., Ganeshram, R., 2015. New insights into productivity and redox-controlled trace element (Ag, Cd, Re, and Mo) accumulation in a 55 kyr long sediment record from Guaymas Basin, Gulf of California. *Paleoceanography* 30 (2), 77–94.
- Chapman, P., Shannon, L.V., 1985. The Benguela ecosystem. II: Chemistry and related processes. *Oceanogr. Marine Biol.* 23, 183–251.
- Cofrancesco, J., 2016. Geochemical signatures for redepositional environments beneath oxygen minimum zones: the Benguela upwelling system offshore Namibia M.S. thesis. Oklahoma State University.
- Collier, R.W., 1985. Molybdenum in the Northeast Pacific Ocean I. *Limnol. Oceanogr.* 30 (6), 1351–1354.
- Cruse, A., Lyons, T., 2004. Trace metal records of regional paleoenvironmental variability in Pennsylvanian (Upper Carboniferous) black shales. *Chem. Geol.* 206 (3), 319–345.
- Crusius, J., Thomson, J., 2003. Mobility of authigenic rhodium, silver, and selenium during postdepositional oxidation in marine sediments. *Geochim. Cosmochim. Acta* 67 (2), 265–273. [https://doi.org/10.1016/S0016-7037\(02\)01075-X](https://doi.org/10.1016/S0016-7037(02)01075-X).
- Crusius, J., Calvert, S., Pedersen, T., Sage, D., 1996. Rhodium and molybdenum enrichments in sediments as indicators of oxic, suboxic and sulfidic conditions of deposition. *Earth Planet. Sci. Lett.* 145 (1), 65–78.
- Demaison, G.J., Moore, G.T., 1980. Anoxic environments and oil source bed genesis. *AAPG Bull.* 64 (8), 1179–1209.
- Dymond, J., Suess, E., Lyle, M., 1992. Barium in deep-sea sediment: A geochemical proxy for paleoproductivity. *Paleoceanography* 7, 163–181.
- Dyrssen, D., Kremling, K., 1990. Increasing hydrogen sulphide concentrations and trace metal behaviour in the anoxic Baltic waters. *Mar. Chem.* 30, 193–204. [https://doi.org/10.1016/0304-4203\(90\)90070-S](https://doi.org/10.1016/0304-4203(90)90070-S).
- Emerson, S., Husted, S., 1991. Ocean anoxia and the concentrations of molybdenum and vanadium in seawater. *Mar. Chem.* 34 (3), 177–196.
- Erickson, B.E., Helz, G.R., 2000. Molybdenum (VI) speciation in sulfidic waters: Stability and lability of thiomolybdates. *Geochim. Cosmochim. Acta* 64 (7), 1149–1158. [https://doi.org/10.1016/S0016-7037\(99\)00423-8](https://doi.org/10.1016/S0016-7037(99)00423-8).
- Fisher, N.S., Wente, M., 1993. The release of trace elements by dying marine phytoplankton. *Deep-Sea Research* 140, 671–694.
- Flegel, A.R., Sanudo-Wilhelmy, S.A., Scelfo, G.M., 1995. Silver in the eastern Atlantic Ocean. *Mar. Chem.* 49 (4), 315–320.
- Formolo, M.J., Riedinger, N., Gill, B.C., 2014. Geochemical evidence for euxinia during the late Devonian extinction events in the Michigan Basin (USA). *Palaeogeogr. Palaeoclimatol. Palaeoecol.* 414, 146–154. <https://doi.org/10.1016/j.palaeo.2014.08.024>.
- Friedl, G., Pedersen, T.F., 1998. Silver as a palaeo proxy for high productivity. *Mineralogical Magazine* 62A, 476–477. Part I. <https://doi.org/10.1180/minmag.1998.62A.1.252>.
- Friedl, G., Pedersen, T.F., 2001. Silver as a new tracer for diatom production. *EAWAG News* 52 (D), 14–15.
- Froelich, P., Klinkhammer, G.P., Bender, M.L., Luedtke, N.A., Heath, G.R., Cullen, D., Dauphin, P., Hammond, D., Hartman, B., Maynard, V., 1979. Early oxidation of organic matter in pelagic sediments of the eastern equatorial Atlantic: suboxic diagenesis. *Geochim. Cosmochim. Acta* 43, 1075–1090.
- Gill, B.C., Lyons, T.W., Young, S.A., Kump, L.R., Knoll, A.H., Saltzman, M.R., 2011. Geochemical evidence for widespread euxinia in the later Cambrian Ocean. *Nature* 469, 80–83. <https://doi.org/10.1038/nature09700>.
- Giraudeau, J., Monteiro, P., Nikodemus, K., 1993. Distribution and malformation of living coccolithophores in the northern Benguela upwelling system off Namibia. *Mar. Micropaleontol.* 22 (1), 93–110.
- Giraudeau, J., Bailey, G.W., Pujol, C., 2000. A high-resolution time-series analyses of particle fluxes in the Northern Benguela coastal upwelling system: carbonate record of changes in biogenic production and particle transfer processes. *Deep-Sea Res. II Top. Stud. Oceanogr.* 47 (9–11), 1999–2028. [https://doi.org/10.1016/S0967-0645\(00\)00014-X](https://doi.org/10.1016/S0967-0645(00)00014-X).
- Goldammer, T., Brunner, B., Bernasconi, S.M., Ferdelman, T.G., Zabel, M., 2011. Phosphate oxygen isotopes: insights into sedimentary phosphorus cycling from the Benguela upwelling system. *Geochim. Cosmochim. Acta* 75 (13), 3741–3756.
- Goldschmidt, V. M. (1954) *Geochemistry* (Vol. 78, no. 2, p. 156). LWW.
- Helz, G., Miller, C., Charnock, J., Mosselmann, J., Patrick, R., Garner, C., Vaughan, D., 1996. Mechanism of molybdenum removal from the sea and its concentration in black shales: EXAFS evidence. *Geochim. Cosmochim. Acta* 60 (19), 3631–3642.
- Helz, G.R., Bura-Nakić, E., Mikac, N., Ciglencić, I., 2011. New model for molybdenum behavior in euxinic waters. *Chem. Geol.* 284 (3–4), 323–332.
- Hendy, I.L., Pedersen, T.F., 2005. Is pore water oxygen content decoupled from productivity on the California margin? Trace element results from Ocean Drilling Program Hole 1017E, San Lucia slope, California. *Paleoceanography* 20 (4). <https://doi.org/10.1029/2004PA001123>.
- Horner, T.J., Kinsley, C.W., Nielsen, S.G., 2015. Barium-isotopic fractionation in seawater mediated by barite cycling and oceanic circulation. *Earth Planet. Sci. Lett.* 430, 511–522. <https://doi.org/10.1016/j.epsl.2015.07.027>.
- Huerta-Diaz, M.A., Morse, J.W., 1990. A quantitative method for determination of trace metal concentration in sedimentary pyrite. *Mar. Chem.* 29, 119–144.
- Huerta-Diaz, M.A., Morse, J.W., 1992. The pyritization of trace metals in anoxic marine sediments. *Geochim. Cosmochim. Acta* 56, 2681–2702.
- Inthorn, M., Mohrholz, V., Zabel, M., 2006a. Nepheloid layer distribution in the Benguela upwelling area offshore Namibia. *Deep-Sea Res. I Oceanogr. Res. Pap.* 53 (8), 1423–1438.
- Inthorn, M., Wagner, T., Scheeder, G., Zabel, M., 2006b. Lateral transport controls distribution, quality, and burial of organic matter along continental slopes in high-productivity areas. *Geology* 34 (3), 205–208.
- Jenkyns, H.C., 2010. Geochemistry of oceanic anoxic events. *Geochim. Geophys. Geosyst.*

- 11 (3).
- Klump, J., Hebbeln, D., Wefer, G., 2000. The impact of sediment provenance on barium-based productivity estimates. *Mar. Geol.* 169, 259–271. [https://doi.org/10.1016/S0025-3227\(00\)00092-X](https://doi.org/10.1016/S0025-3227(00)00092-X).
- Kowalski, N., Dellwig, O., Beck, M., Gräwe, U., Neubert, N., Nägler, T.F., Badewien, H., Brumsack, H.-J., van Beusekom, J.E.E., Böttcher, M.E., 2013. Pelagic molybdenum concentration anomalies and the impact of sediment resuspension on the molybdenum budget in two tidal systems of the North Sea. *Geochim. Cosmochim. Acta* 119, 198–211.
- Kristensen, E., 2000. Organic matter diagenesis at the oxic/anoxic interface in coastal marine sediments, with emphasis on the role of burrowing animals. In: *Life at Interfaces and under Extreme Conditions*. Springer, Dordrecht, pp. 1–24.
- Lipinski, M., Warning, B., Brumsack, H.J., 2003. Trace metal signatures of Jurassic/cretaceous black shales from the Norwegian Shelf and the Barents Sea. *Palaeogeogr. Palaeoclimatol. Palaeoecol.* 190, 459–475.
- Little, S.H., Vance, D., Lyons, T.W., McManus, J., 2015. Controls on trace metal authigenic enrichment in reducing sediments: insights from modern oxygen-deficient settings. *Am. J. Sci.* 315 (2), 77–119.
- Lüning, S., Kolonic, S., 2003. Uranium spectral gamma-ray response as a proxy for organic richness in black shales: Applicability and limitations. *J. Pet. Geol.* 26 (2), 153–174.
- Lyons, T.W., Severmann, S., 2006. A critical look at iron paleoredox proxies: New insights from modern euxinic marine basins. *Geochim. Cosmochim. Acta* 70 (23), 5698–5722.
- Lyons, T.W., Werne, J.P., Hollander, D.J., Murray, R.W., 2003. Contrasting sulfur geochemistry and Fe/Al and Mo/Al ratios across the last oxic-to-anoxic transition in the Cariaco Basin, Venezuela. *Chem. Geol.* 195 (1–4), 131–157.
- Lyons, T.W., Anbar, A.D., Severmann, S., Scott, C., Gill, B.C., 2009. Tracking euxinia in the ancient ocean: a multiproxy perspective and Proterozoic case study. *Annu. Rev. Earth Planet. Sci.* 37, 507–534.
- Martin, J.H., Knauer, G.A., Gordon, R.M., 1983. Silver distributions and fluxes in north-east Pacific waters. *Nature* 305 (5932), 306–309.
- McBride, M.B., 1979. Mobility and reactions of VO^{2+} on hydrated smectite surfaces. *Clay Miner.* 27, 91–96.
- McKay, J.L., Pedersen, T.F., 2008. The accumulation of silver in marine sediments: a link to biogenic Ba and marine productivity. *Glob. Biogeochem. Cycles* 22, GB4010. <https://doi.org/10.1029/2007GB003136>.
- McManus, J., Berelson, W.M., Klinkhammer, G.P., Kilgore, T.E., Hammond, D.E., 1994. Remobilization of barium in continental margin sediments. *Geochimica et Cosmochimica Acta* 58 (22), 4899–4907.
- McPhee-Shaw, E.E., Sternberg, R.W., Mullenbach, B., Ogston, A.S., 2004. Observations of intermediate nepheloid layers on the northern California continental margin. *Cont. Shelf Res.* 24, 693–720.
- Mollenhauer, G., Schneider, R.R., Müller, P.J., Spieß, V., Wefer, G., 2002. Glacial/interglacial variability in the Benguela upwelling system: Spatial distribution and budgets of organic carbon accumulation. *Glob. Biogeochem. Cycles* 16 (4).
- Mollenhauer, G., Inthorn, M., Vogt, T., Zabel, M., Damsté, J., Eglinton, T., 2007. Aging of marine organic matter during cross-shelf lateral transport in the Benguela upwelling system revealed by compound-specific radiocarbon dating. *Geochem. Geophys. Geosys.* 8 (9).
- Monteiro, P.M.S., Van der Plas, A., Mohrholz, V., Mabilhe, E., Pascall, A., Joubert, W., 2006. Variability of natural hypoxia and methane in a coastal upwelling system: Oceanic physics or shelf biology? *Geophys. Res. Lett.* 33 (16).
- Moore, J.N., Ficklin, W.H., Johns, C., 1988. Partitioning of arsenic and metals in reducing sulfidic sediments. *Environ. Sci. Technol.* 22 (4), 432–437.
- Morford, J.L., Emerson, S., 1999. The geochemistry of redox sensitive trace metals in sediments. *Geochim. Cosmochim. Acta* 63, 1735–1750.
- Morford, J.L., Kalnejais, L.H., Helman, P., Yen, G., Reinard, M., 2008. Geochemical cycling of silver in marine sediments along an offshore transect. *Mar. Chem.* 110, 77–88.
- Morse, J., Luther, G., 1999. Chemical influences on trace metal-sulfide interactions in anoxic sediments. *Geochim. Cosmochim. Acta* 63 (19), 3373–3378.
- Nameroff, T., 1996. The geochemistry of redox-sensitive metals in sediments of the oxygen minimum off Mexico (Doctoral dissertation, Ph. D. thesis, Univ. of Wash., Seattle).
- Nameroff, T., Balistrieri, L., Murray, J., 2002. Suboxic trace metal geochemistry in the eastern tropical North Pacific. *Geochim. Cosmochim. Acta* 66 (7), 1139–1158.
- Owens, J.D., Reinhard, C.T., Rohrsen, M., Love, G.D., Lyons, T.W., 2016. Empirical links between trace metal cycling and marine microbial ecology during a large perturbation to Earth's carbon cycle. *Earth Planet. Sci. Lett.* 449, 407–417.
- Owens, J.D., Lyons, T.W., Hardisty, D.S., Lowery, C.M., Lu, Z., Lee, B., Jenkyns, H.C., 2017. Patterns of local and global redox variability during the Cenomanian-Turonian Boundary Event (Oceanic Anoxic Event 2) recorded in carbonates and shales from Central Italy. *Sedimentology* 64, 168–185.
- Piper, D., Calvert, S., 2009. A marine biogeochemical perspective on black shale deposition. *Earth Sci. Rev.* 95 (1), 63–96.
- Piper, D.Z., Perkins, R.B., 2004. A modern vs. Permian black shale—the hydrography, primary productivity, and water-column chemistry of deposition. *Chem. Geol.* 206 (3–4), 177–197. <https://doi.org/10.1016/j.chemgeo.2003.12.006>.
- Poulson Brucker, R.L., McManus, J., Severmann, S., Berelson, W.M., 2009. Molybdenum behavior during early diagenesis: Insights from Mo isotopes. *Geochem. Geophys. Geosyst.* 10 (6). <https://doi.org/10.1029/2008GC002180>.
- Raiswell, R., Berner, R.A., 1985. Pyrite formation in euxinic and semi-euxinic sediments. *Am. J. Sci.* 285, 710–724.
- Raiswell, R., Canfield, D., 2012. The iron biogeochemical cycle past and present. *Geochem. Perspect.* 1 (1), 1–2.
- Raiswell, R., Hardisty, D.S., Lyons, T.W., Canfield, D.E., Owens, J.D., Planavsky, N.J., Poulton, S.W., Reinhard, C.T., 2018. The iron paleoredox proxies: a guide to the pitfalls, problems and proper practice. *Am. J. Sci.* 318 (5), 491–526.
- Reinhard, C.T., Planavsky, N.J., Robbins, L.J., Partin, C.A., Gill, B.C., Lalonde, S.V., Bekker, A., Konhauser, K.O., Lyons, T.W., 2013. Proterozoic Ocean redox and biogeochemical stasis. *Proc. Natl. Acad. Sci.* 110 (14), 5357–5362. <https://doi.org/10.1073/pnas.1208622110>.
- Resing, J.A., Sedwick, P.N., German, C.R., Jenkins, W.J., Moffett, J.W., Sohst, B.M., Tagliabue, A., 2015. Basin-scale transport of hydrothermal dissolved metals across the South Pacific Ocean. *Nature* 523 (7559), 200–203. <https://doi.org/10.1038/nature14577>.
- Riedinger, N., Kasten, S., Gröger, J., Franke, C., Pfeifer, K., 2006. Active and buried authigenic barite fronts in sediments from the Eastern Cape Basin. *Earth Planet. Sci. Lett.* 241, 876–887. <https://doi.org/10.1016/j.epsl.2005.10.032>.
- Röhl, H.J., Schmid-Röhl, A., Oschmann, W., Frimmel, A., Schwark, L., 2001. The Posidonia Shale (lower Toarcian) of SW-Germany: an oxygen-depleted ecosystem controlled by sea level and palaeoclimate. *Palaeogeogr. Palaeoclimatol. Palaeoecol.* 165 (1–2), 27–52.
- Sahoo, S.K., Planavsky, N.J., Jiang, G., Kendall, B., Owens, J.D., Wang, X., Shi, X., Anbar, A.D., Lyons, T.W., 2016. Oceanic oxygenation events on the anoxic Ediacaran Ocean. *Geobiology* 14, 457–468.
- Saito, M.A., Noble, A.E., Tagliabue, A., Goepfert, T.J., Lamborg, C.H., Jenkins, W.J., 2013. Slow-spreading submarine ridges in the South Atlantic as a significant oceanic iron source. *Nat. Geosci.* 6 (9), 775–779.
- Schmidtko, S., Stramma, L., Visbeck, M., 2017. Decline in global oceanic oxygen content during the past five decades. *Nature* 542, 335–339.
- Scholz, F., 2018. Identifying oxygen minimum zone-type biogeochemical cycling in Earth history using inorganic geochemical proxies. *Earth Sci. Rev.* 184, 29–45.
- Scholz, F., Hensen, C., Noffke, A., Rohde, A., Liebetrau, V., Wallmann, K., 2011. Early diagenesis of redox-sensitive trace metals in the Peru upwelling area—response to ENSO-related oxygen fluctuations in the water column. *Geochim. Cosmochim. Acta* 75 (22), 7257–7276.
- Scholz, F., Severmann, S., McManus, J., Hensen, C., 2014. Beyond the Black Sea paradigm: the sedimentary fingerprint of an open-marine iron shuttle. *Geochim. Cosmochim. Acta* 127, 368–380.
- Scott, C., Lyons, T., 2012. Contrasting molybdenum cycling and isotopic properties in euxinic versus non-euxinic sediments and sedimentary rocks: refining the paleoproxies. *Chem. Geol.* 324–325, 19–27.
- Scott, C., Slack, J.F., Kelley, K.D., 2017. The hyper-enrichment of V and Zn in black shales of the late Devonian-early Mississippian Bakken formation (USA). *Chem. Geol.* 452, 24–33.
- Seeberg-Elverfeldt, J., Schlüter, M., Feseker, T., Kölling, M., 2005. Rhizon sampling of pore waters near the sediment/water interface of aquatic systems. *Limnol. Oceanogr. Methods* 3 (8), 361–371.
- Severmann, S., Lyons, T.W., Anbar, A., McManus, J., Gordon, G., 2008. Modern iron isotope perspective on the benthic iron shuttle and the redox evolution of ancient oceans. *Geology* 36 (6), 487–490. <https://doi.org/10.1130/G24670A.1>.
- Severmann, S., McManus, J., Berelson, W.M., Hammond, D.E., 2010. The continental shelf benthic iron flux and its isotopic composition. *Geochim. Cosmochim. Acta* 74, 3984–4004. <https://doi.org/10.1016/j.gca.2010.04.022>.
- Shannon, L.V., Nelson, G., 1996. The Benguela: large scale features and processes and system variability. In: *The South Atlantic*. Springer, Berlin, Heidelberg, pp. 163–210.
- Shaw, T.J., Gieskes, J.M., Jahnke, R.A., 1990. Early diagenesis in differing depositional environments: the response of transition metals in pore water. *Geochim. Cosmochim. Acta* 54, 1233–1246.
- Steinmann, J.W., Grammer, G.M., Brunner, B., Jones, C.K., Riedinger, N., 2020. Assessing the application of trace metals as paleoproxies and a chemostratigraphic tool in carbonate systems: a case study from the “Mississippian Limestone” of the mid-continent, United States. *Mar. Pet. Geol.* 112, 104061.
- Stramma, L., Johnson, G.C., Sprintall, J., Mohrholz, V., 2008. Expanding oxygen-minimum zones in the tropical oceans. *Science* 320, 655–658. <https://doi.org/10.1126/science.1153847>.
- Summerhayes, C., Kroon, D., Rosell-Melé, A., Jordan, R., Schrader, H., Hearn, J., Villanueva, J., Grimalt, G., Eglinton, G., 1995. Variability in the Benguela current upwelling system over the past 70,000 years. *Prog. Oceanogr.* 35 (3), 207–251.
- Them, T.R., Gill, B.C., Selby, D., Gröcke, D.R., Friedman, R.M., Owens, J.D., 2017. Evidence for rapid weathering response to climatic warming during the Toarcian Oceanic Anoxic Event. *Sci. Rep.* 7 (1), 1–10.
- Torres, M.E., Brumsack, H.J., Bohrmann, G., Emeis, K.C., 1996. Barite fronts in continental margin sediments: a new look at barium remobilization in the zone of sulfate reduction and formation of heavy barites in diagenetic fronts. *Chem. Geol.* 127 (1–3), 125–139. [https://doi.org/10.1016/0009-2541\(95\)00090-9](https://doi.org/10.1016/0009-2541(95)00090-9).
- Tribouillard, N., Ribouilleau, A., Lyons, T.W., Baudin, F., 2004. Enhanced trapping of molybdenum by sulfurized organic matter of marine origin as recorded by various Mesozoic formations. *Chem. Geol.* 213, 385–401.
- Tribouillard, N., Ramdani, A., Trentesaux, A., 2005. Controls on organic accumulation in Late Jurassic shales of northwestern Europe as inferred from trace-metal geochemistry. In: Harris, N. (Ed.), *The Deposition of Organic-Carbon-Rich Sediments: Models, Mechanisms, and Consequences*. 82. SEPM Special Publication, pp. 145–164.
- Tribouillard, N., Algeo, T., Lyons, T., Ribouilleau, A., 2006. Trace metals as paleoredox and paleoproductivity proxies: an update. *Chem. Geol.* 232 (1), 12–32.
- Turekian, K.K., Wedepohl, K.H., 1961. Distribution of the elements in some major units of the earth's crust. *Geol. Soc. Am. Bull.* 72 (2), 175–192.
- Tyson, R.V., 1987. The genesis and palynofacies characteristics of marine petroleum source rocks. *Geol. Soc. Lond., Spec. Publ.* 26 (1), 47–67. <https://doi.org/10.1144/GSL.SP.1987.026.01.03>.
- Tyson, R.V., Pearson, T.H., 1991. Modern and ancient continental shelf anoxia: an

- overview. In: Tyson, R.V., Pearson, T.H. (Eds.), *Modern and Ancient Continental Shelf Anoxia*. 58. Geological Society Special Publications, pp. 1–26.
- Van der Sloot, H.A., Hoede, D., Wijkstra, J., Duinker, J.C., Nolting, R.F., 1985. Anionic species of V, As, Se, Mo, Sb, Te and W in the Scheldt and Rhine estuaries and the Southern Bight (North Sea). *Estuar. Coast. Shelf Sci.* 21, 633–651.
- Van der Weijden, C.H., Reichart, G.J., Visser, H.J., 1999. Enhanced preservation of organic matter in sediments deposited within the oxygen minimum zone in the northeastern Arabian Sea. *Deep-Sea Res. I Oceanogr. Res. Pap.* 46, 807–830.
- Volkenborn, N., Hedtkamp, S.I.C., Van Beusekom, J.E.E., Reise, K., 2007. Effects of bioturbation and bioirrigation by lugworms (*Arenicola marina*) on physical and chemical sediment properties and implications for intertidal habitat succession. *Estuar. Coast. Shelf Sci.* 74, 331–343. <https://doi.org/10.1016/j.ecss.2007.05.001>.
- Von Breyman, M.T., Emeis, K.C., Suess, E., 1992. Water depth and diagenetic constraints on the use of barium as a palaeoproductivity indicator. *Geol. Soc. Lond., Spec. Publ.* 64 (1), 273–284.
- Wagner, M., Hendy, I., McKay, J., Pedersen, T., 2013. Influence of biological productivity on silver and redox-sensitive trace metal accumulation in Southern Ocean surface sediments, Pacific sector. *Earth and Planetary Science Letters* 380, 31–40. <https://doi.org/10.1016/j.epsl.2013.08.020>.
- Wanty, R.B., Goldhaber, M.B., 1992. Thermodynamics and kinetics of reactions involving vanadium in natural systems: accumulation of vanadium in sedimentary rocks. *Geochim. Cosmochim. Acta* 56, 1471–1483.
- Wehrli, B., Stumm, W., 1989. Vanadyl in natural waters: adsorption and hydrolysis promote oxygenation. *Geochim. Cosmochim. Acta* 53 (1), 69–77.
- Werne, J.P., Sageman, B.B., Lyons, T.W., Hollander, D.J., 2002. An integrated assessment of a type 'euxinic' deposit: evidence for multiple controls on black shale deposition in the Middle Devonian Oatka Creek Formation. *Am. J. Sci.* 302 (2), 110–143. <https://doi.org/10.2475/ajs.302.2.110>.
- Whitfield, M., 2002. Interactions between phytoplankton and trace metals in the ocean. *Adv. Mar. Biol.* 41, 3–120.
- Wignall, P.B., Myers, K.J., 1988. Interpreting benthic oxygen levels in mudrocks: a new approach. *Geology* 16 (5), 452–455.
- Zheng, Y., Anderson, R.F., Van Geen, A., Kuwabara, J., 2000. Authigenic molybdenum formation in marine sediments: a link to pore water sulfide in the Santa Barbara Basin. *Geochim. Cosmochim. Acta* 64 (24), 4165–4178.
- Zhu, B., Jiang, S., Pi, D., Ge, L., Yang, J., 2018. Trace elements Characteristics of Black Shales from the Ediacaran Doushantuo Formation, Hubei Province, South China: Implications for Redox and Open vs. Restricted Basin Conditions. *J. Earth Sci.* 29 (2), 342–352. <https://doi.org/10.1007/s12583-017-0907-5>.